



# Novel perovskite nanocatalyst (BiFeO<sub>3</sub>) for the photodegradation of rhodamine B/tartrazine and swift reduction of nitro compounds

Harinder Singh<sup>1</sup> · Jaspreet Kaur Rajput<sup>1</sup>

Received: 29 January 2019 / Accepted: 6 June 2019  
© Iranian Chemical Society 2019

## Abstract

Design and synthesis of visible light respondent photocatalyst with high separation efficiency is of great importance due to its application in practical point of view. In this presentation, novel perovskite-structured BiFeO<sub>3</sub> nanoparticles have been successfully synthesized by simple, cost-effective and eco-friendly technique. The BiFeO<sub>3</sub> nanoparticles were prepared by using different chelating agents (sucrose, citric acid, tartaric acid and urea) and under different range of calcination temperature (150–850 °C). Different characterization techniques such as FT-IR, XRD, VSM, BET, TEM and UV–Vis spectroscopy have been used for its structure evaluation. Further, by using this catalyst, a green approach has been developed for the removal of harmful organic compounds from the industrial waste. The catalytic activity was assessed by the catalytic degradation of industrial waste dyes such as rhodamine B and tartrazine (first time by perovskite-structured material) in aqueous media under sunlight irradiation and reduction of various nitro compounds to corresponding amines (in s) by using NaBH<sub>4</sub> in green solvent water at room temperature. Effect of all types of BiFeO<sub>3</sub> nanoparticles on catalytic degradation and reduction was investigated. BiFeO<sub>3</sub> nanoparticles prepared by sucrose as chelating agent and calcinated at 650° were selected as a better catalyst on the basis of its performance in degradation and reduction experiment. Thus, the present approach provides a promising way to prepare noble catalyst for extensive applications in degradation/reduction of organic pollutants. The examination of degraded products of dye has been carried out by using FT-IR; mass spectroscopy and UV–Vis spectroscopy and confirmation of reduction of nitrocompounds with UV–Vis spectroscopy.

**Keywords** RhB · Tartrazine · Degradation · Reduction · Photocatalyst · BiFeO<sub>3</sub>

## Introduction

Environmental pollution is the area of great concern of twenty-first century. Waste coming out from textile and dye industries is very hazardous to living bodies on earth [1]. Nearly, 1–20% of dyes are released as textile effluents of the total world production of dyes during dyeing process [2]. Various organic dyes which are water soluble are used in various industries, and their degraded products represent a series of environmental issue [3] for human beings because

they display high toxicity, slow biodegradation, low decoloration [2], prospective mutagenic and carcinogenic effects [4]. Even a very small concentration of the dyes in effluents coming out from industries is highly visible and undesirable. The colored part reduces the transparency, which reduces the penetration of light, and results in the obstruction of the photosynthesis and responsible for the destruction of large number of water living organisms. Rhodamine B is a basic dye of xanthene class, extensively used as colorant in textiles and food stuffs. It is extremely soluble in water and organic solvents and is well known as water tracer fluorescent. Due to its terrible health effects such as irritation of skin, eyes and respiratory track, it is declared as harmful to human and animal life. Further its neurotoxicity, carcinogenicity, development toxicity, chronic toxicity, and reproductive toxicity have proven experimentally for both humans and animals [5, 6]. Tartrazine is an azo dye also known as FD&C Yellow No. 5, widely used in food coloring, cosmetics, drugs, etc., and present in maximum amount in industrial effluents cause

**Electronic supplementary material** The online version of this article (<https://doi.org/10.1007/s13738-019-01710-6>) contains supplementary material, which is available to authorized users.

✉ Harinder Singh  
Harindersingh87@gmail.com

<sup>1</sup> Department of Chemistry, Dr. B R Ambedkar National Institute of Technology, Jalandhar, Punjab 144011, India

various health issues for humans such as allergic reactions among hypersensitive persons. It causes headaches, hives, insomnia, asthma attack, thyroid cancer and lupus [7, 8]. Therefore, the elimination of organic dyes from environment attracted much interest in the past decades.

Various methods like physical (adsorption, ultra filtration, coagulation and ion exchange) and biological (bacteria and yeasts) have been reported in the literature so far, for the elimination of colored effluents coming out with industrial and textile waste. These methods are not successful complete for the conversion of contaminants into less harmful and useful products [9, 10]. Moreover, they do not cause the complete degradation and also unable to stop their movement from one phase to another. These methods do not work well due to high stability and resistance to chemical and biological degradation of dyes. So, more convenient method is still in demand which overcomes these problems for the waste water treatment [11].

Nowadays, photocatalysis is proven to be more convenient, simple and eco-friendly way for the degradation of harmful dyes due to the use of oxygen as oxidant, low-temperature oxidation of organic compounds and complete mineralization.  $\text{TiO}_2$  is reported to degrade many organic dyes under UV irradiation. However, its large band gap ( $\sim 3.2$  eV) restricts its application as photocatalyst in visible light [12]. The sunlight consists of less than 4% of UV light and more than 50% of the visible light. Hence, the development of non-titania catalyst with high catalytic activity in visible region with narrow band gap is highly desirable [2].

Due to the environmental conditions of India, the sunlight is abundantly available throughout the year. So the harmful dyes can be degraded easily using natural sources of light by using photocatalyst [5]. The photodegradation of tartrazine and rhodamine B has been carried out under sunlight by using  $\text{BiFeO}_3$  as an efficient and cost-effective catalyst.

Aromatic nitro compounds are used in various industries for the formation of fungicides, rubber, insecticides and synthetic dyes [13, 14]. Their solubility and stability in aqueous media make it a serious issue of environmental pollution, referred as the main pollutant coming out from chemical, drug industries and agriculture waste. Its serious inhalation causes nausea, drowsiness, headaches, cyanosis and eye irritation [15]. So its quick degradation is required. The simple and cost-effective method is to convert them in aromatic amines through reduction by using  $\text{NaBH}_4$  as a reducing agent. Thus, its reduction to amino compounds is of high importance [16]. Because aromatic amines are the important starting materials or intermediates or precursors for the formation of the pigments, pharmaceuticals products, herbicides, polymers, dye stuffs, surfactants, agricultural chemical [17, 18] and used as a photographic developer, lubricating and anticorrosion agent [16]. Various reducing

agents, numerous catalysts [16–20] and methodologies [21] are available for this transformation but all of them have limitations such as prolonged reaction time, high  $\text{H}_2$  pressure, use of organic solvents, reduced recyclability and high temperature. So the development of proficient and consistent technique is highly desirable for the reduction of ANCs (aromatic nitro compounds). Among reducing agents,  $\text{NaBH}_4$  is of high important, since it is milder, selective and thermally stable chemical hydride [20]. It represents the best economical option for the reduction reactions at normal conditions of temperature and pressure.

Perovskite-structured  $\text{BiFeO}_3$  nanoparticles have got much attention due to its high chemical and thermal stability, potential electronic and magnetic applications [12]. In addition, narrow band-gap energy (2.1 eV) and photovoltaic effects show their tendency to act as photocatalyst under visible light for degradation of harmful industrial compounds [22]. All these observations make them a promising photocatalyst by utilizing solar energy for purification of waste water [12].

The present work aims to provide a new-generation hybrid system with high catalytic efficiency and stability. Here we reported the potentiality of the  $\text{BiFeO}_3$  nanoparticles as heterogeneous photocatalyst that has been investigated for the degradation of RhB and tartrazine (first time ever) in aqueous media under sunlight irradiation and for the reduction of ANCs (aromatic nitro compounds) in aqueous media at room temperature. In addition to excellent catalytic activity of the as-prepared catalyst, it could be easily recovered from the reaction medium by using an external magnet and reused up to five times without considerable loss in activity, indicative of its potential application in chemical industries.

## Experimental section

### Materials

Bismuth nitrate (pentahydrate), ferric nitrate (extra pure, nonahydrate), tartaric acid (extra pure), sucrose (extra pure), citric acid (pure) and urea were purchased from Loba Chemie. Nitric acid (70%) was supplied by Merck. 4-nitrophenol, 2-nitrophenol, 2, 4-dinitrophenol, 4-nitroaniline, 2-nitroaniline and 2,4-dinitroaniline were supplied by Avra synthesis. All these were used as such without any further purification.

### Methods

The crystal structure of prepared magnetic nanoparticles catalyst was investigated by X-ray diffraction (XRD) using a Panlytical XPERTPRO (NPD) X-ray diffractometer with

Cu K $\alpha$  radiation ( $\lambda = 0.154$  nm), in the  $2\theta$  range  $10^\circ$ – $80^\circ$ . Fourier transform IR (FT-IR) spectroscopy was carried out by using Agilent Cary 600 in the range  $400$ – $4000$   $\text{cm}^{-1}$ . The morphology was studied using transmission electron microscopy (TEM). The sample was prepared by dispersion of nanoparticles in ethanol, which were deposited on a carbon-coated Cu grid, and after drying, analysis was performed using a Hitachi S7500 instrument. The magnetic properties were measured using a vibrating sample magnetometer (VSM, Princeton Applied Research model 155) at room temperature with a maximum magnetic field range of  $+1$  T to  $-1$  T. Light intensity is measured by digital lux meter of HTC<sup>TM</sup> of model LX-101A. A photocatalytic chamber containing Hg lamp of power 15 W was used as a source of artificial UV irradiation, and the distance of dye solution (when stagnant) was set as 50 cm from the lamp. Ultra-sonic cleaner (sonication) of JSGW model number 1236/2, of  $33 \pm 3$  kHz frequency with internal dimensions  $228 \times 140 \times 100$  mm was used. Surface area and pore characteristics were characterized using Quanta Chrome Nova-1000 surface analyzer instrument under liquid nitrogen temperature with vacuum degassing at  $110^\circ\text{C}$  for 3 h. The specific surface area was calculated using the BET equation. Mass spectroscopy was carried out by using XEVO G2-XS QTOF instrument. ChemDraw ultra 8.0 was used for drawing chemical structures.

### Synthesis of BiFeO<sub>3</sub> nanoparticles

BiFeO<sub>3</sub> nanoparticles were synthesized using Bi(NO<sub>3</sub>)<sub>3</sub>·5H<sub>2</sub>O and Fe(NO<sub>3</sub>)<sub>3</sub>·9H<sub>2</sub>O as precursors.

Bi(NO<sub>3</sub>)<sub>3</sub>·5H<sub>2</sub>O (2.5 mmol) and Fe(NO<sub>3</sub>)<sub>3</sub>·9H<sub>2</sub>O (2.5 mmol) were dissolved in 5 ml of distilled water and 10 ml of 3 M HNO<sub>3</sub>, respectively. These solutions were

sonicated for 10 min. Then two solutions were mixed and again sonicated for 15 min. Addition of 5 mmol of chelating agent (sucrose, citric acid, tartaric acid and urea) was carried out to the mixture followed by stirring for 30 min to enable complete dissolution. The contents were then heated on a hot plate at  $100^\circ\text{C}$  for 30 min. Heating resulted in evaporation, auto-ignition followed by evaporation of large quantities of gases, leaving behind black powder. The black powder so obtained was then calcinated separately at different temperatures such as  $150^\circ\text{C}$ ,  $450^\circ\text{C}$ ,  $550^\circ\text{C}$ ,  $650^\circ\text{C}$ ,  $750^\circ\text{C}$  and  $850^\circ\text{C}$ .

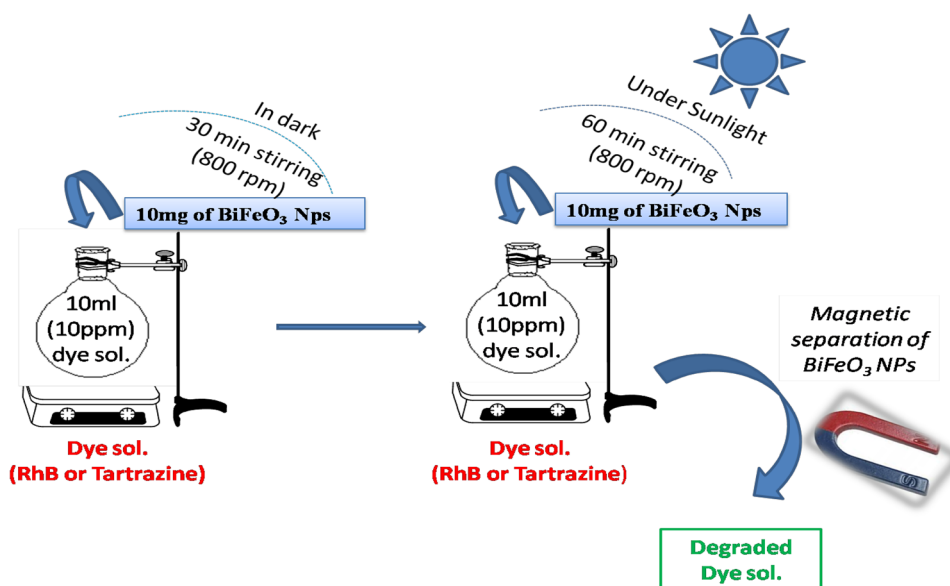
### Sunlight irradiation

In order to estimate the photocatalytic activity of as-synthesized catalyst by auto-combustion route, two different dyes RhB and tartrazine were taken. A typical experiment constitutes 10 ml of 10 ppm of dye solution and 10 mg of catalyst taken in a round-bottom flask. Before exposing to irradiation, the reaction suspension was magnetically stirred at 800 rpm for 30 min in dark to establish adsorption equilibrium between the catalyst and the dye solution. Afterward, the suspension was put under sunlight for appropriate time for complete degradation. The experiments were carried out under direct solar radiation in consecutive sunny days in July, 2017 from 11.30 am to 2.30 pm with an average light intensity 80,000–90,000 Lux. All experiments were carried out under temperature range from  $30$  to  $39^\circ\text{C}$  (Scheme 1).

### Reduction of 4-nitrophenol (NP)

In typical experiment, 5 ml of 4NP (0.1 mmol) was taken; then freshly prepared 12.5 ml of NaBH<sub>4</sub> (0.53 mmol) was added. To the mixture, 25 mg amount of BiFeO<sub>3</sub> was added

**Scheme 1** Photocatalytic degradation of RhB or tartrazine by BiFeO<sub>3</sub> nanoparticles



and the mixture was stirred at 800 rpm at room temperature for appropriate time intervals. The reduction of nitro group to amino group was estimated by elimination of yellow color. The time for decolorization was determined. The reduction phenomena were further investigated by using UV–Vis spectroscopy.

## Results and discussion

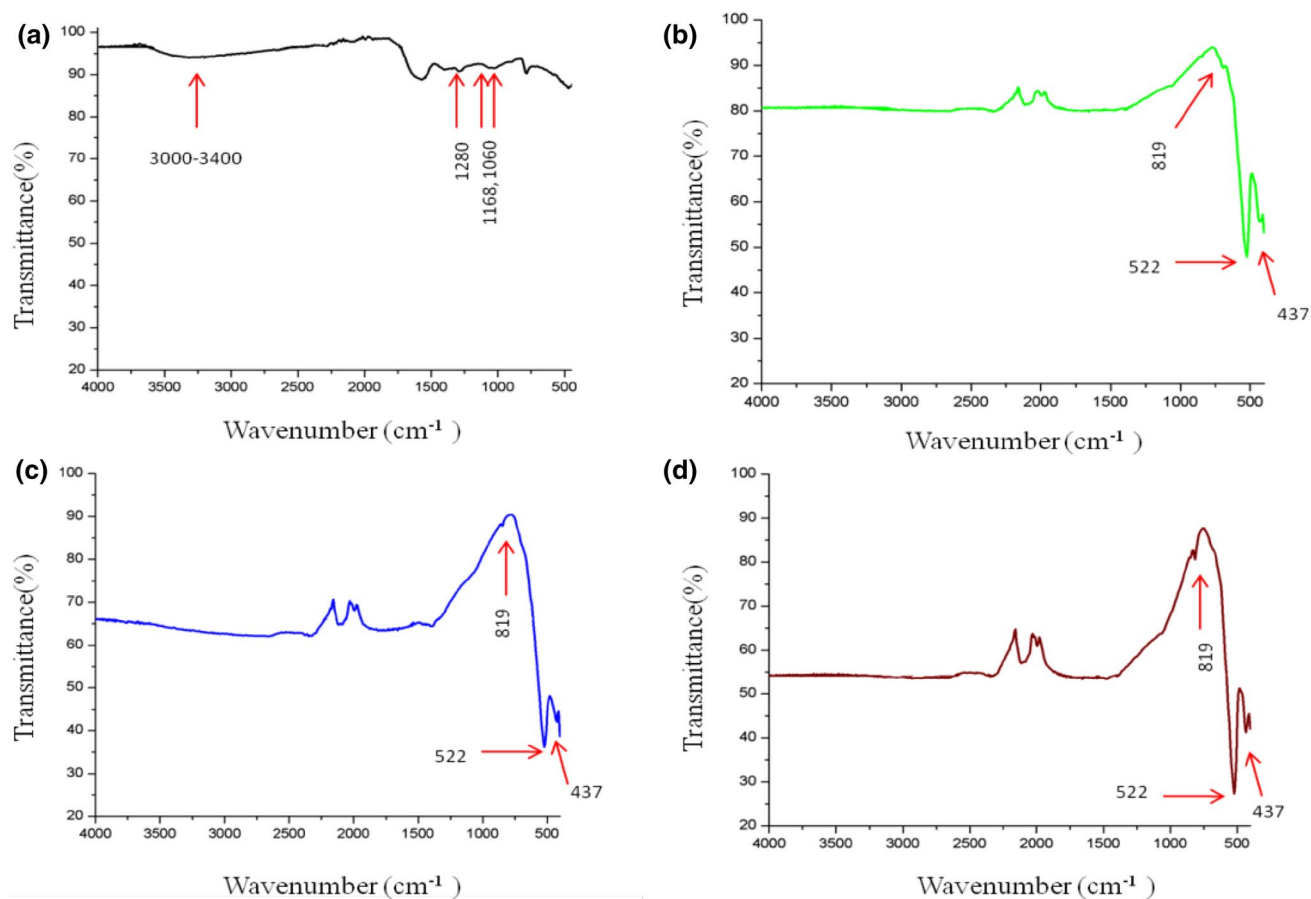
The purpose of adding the chelating agent is to control the size, agglomeration and surface morphology of the nanoparticles. The decomposition of the metal precursor (acting as oxidizer) carried out at normal temperature by using organic fuel (acting as reducing agent) with providing little external heat. During the redox reaction high chemical energy is released which causes the highest level molecular mixing of the components. Sometimes more thermal treatment is needed to remove the organic impurity left in the sample during the course of the reaction. So the selection of chelating agent significantly affects the properties of the nanoparticles [23–25]. In our case, we have used four different chelating agents such as sucrose, citric acid, tartaric

acid and urea and further their effects on degradation and reduction experiment were carried out.

## Characterization of the as-prepared catalyst

### FT-IR

To confirm the removal of organic phase impurities and formation of pure form of  $\text{BiFeO}_3$  nanoparticles prepared by sucrose as chelating agent with increase in calcination temperature, FT-IR analysis was carried out as shown in Fig. 1. In case of calcination temperature  $150^\circ\text{C}$ , a broad peak near  $3000\text{--}3400\text{ cm}^{-1}$  was attributed to the stretching mode of OH of water molecule as the sample might consist of some moisture on its surface and several others peaks observed at  $1060\text{ cm}^{-1}$ ,  $1139\text{ cm}^{-1}$  and  $1165\text{ cm}^{-1}$  were came out from the result of stretching mode of C–OH and C–O–C bond, respectively. With increase in temperature, i.e.,  $450^\circ\text{C}$  and  $550^\circ\text{C}$ , the elimination of such above-mentioned peaks goes on decreasing and FT-IR pattern of sample calcination at highest temperature, i.e.,  $650^\circ\text{C}$  was totally free of such kinds of impurity peaks. Further the formation of new peaks of stretching mode of Bi–O, Fe–O and O–Fe–O bonds of



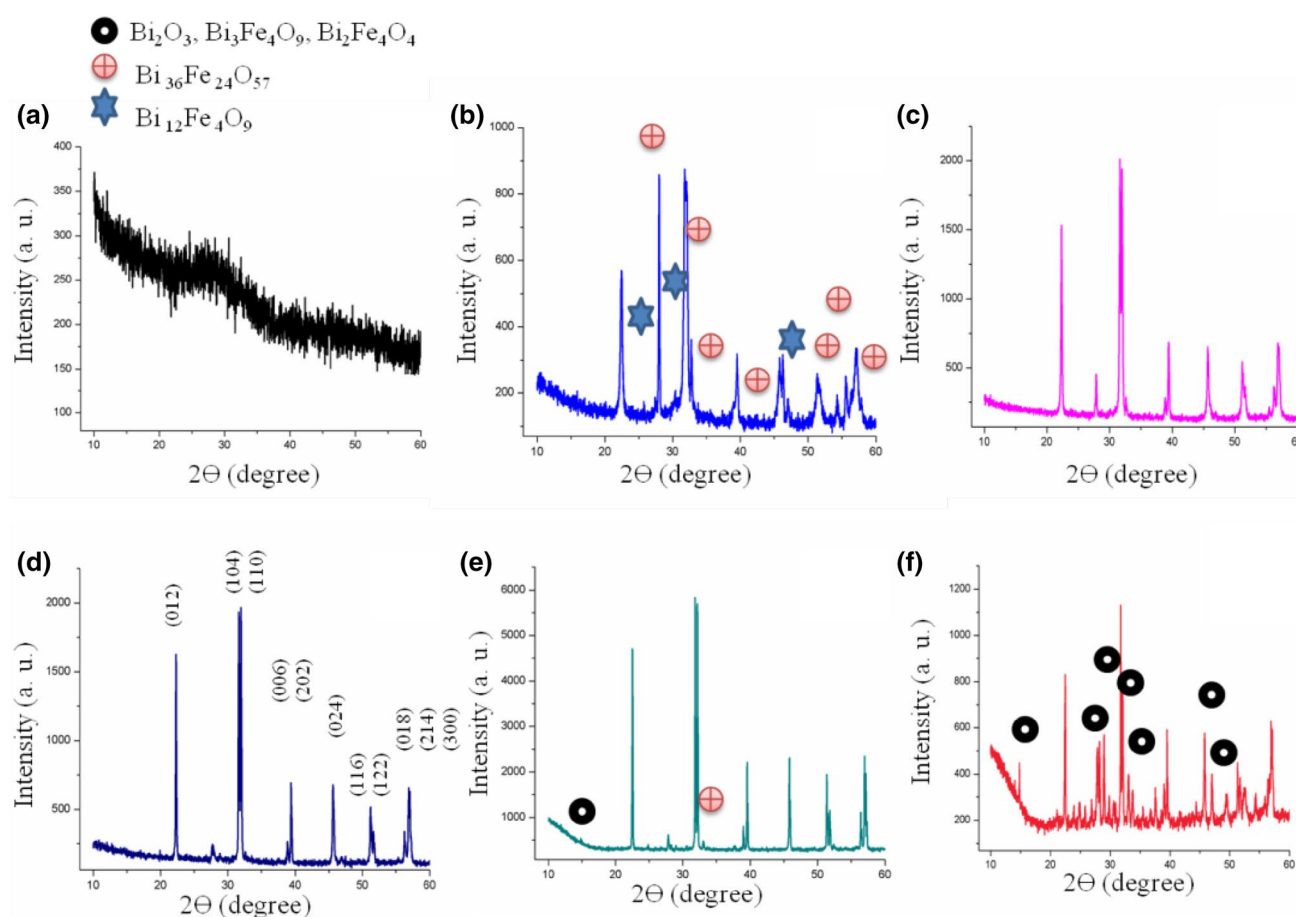
**Fig. 1** Comparison study of FT-IR spectra of  $\text{BiFeO}_3$  calcinated at **a**  $150^\circ\text{C}$ , **b**  $450^\circ\text{C}$ , **c**  $550^\circ\text{C}$  and **d**  $650^\circ\text{C}$

$\text{FeO}_6$  at  $819\text{ cm}^{-1}$ ,  $522\text{ cm}^{-1}$  and  $437\text{ cm}^{-1}$ , respectively [26, 27], was increased with increase in calcination temperature, i.e., sharpness of formation of such peaks increased with from 150 to  $650\text{ }^\circ\text{C}$ , showing the degree of crystallinity increased with increase in calcination temperature [28]. So, calcination temperature  $650\text{ }^\circ\text{C}$  was optimized temperature which was free from all impurity peaks and consists of sharp purity peaks. Therefore, it was considered to be the final calcination temperature to obtain pure form of  $\text{BiFeO}_3$  nanoparticles.

## XRD

For the detection of formation of pure form of  $\text{BiFeO}_3$  nanoparticles using sucrose as chelating agent, XRD analysis of samples calcinated at various temperatures has been explored as depicted in Fig. 2. The material looks like an amorphous in nature with no characteristic peak observed at initial calcination temperature  $150\text{ }^\circ\text{C}$ . Then we increased the calcination temperature to  $450\text{ }^\circ\text{C}$ ,  $550\text{ }^\circ\text{C}$  and  $650\text{ }^\circ\text{C}$  to obtain the pure form of  $\text{BiFeO}_3$  nanoparticles. In case of calcination temperature  $450\text{ }^\circ\text{C}$ , it has been observed that

main peaks of  $\text{BiFeO}_3$  nanoparticles started appearing along with other secondary phases of  $\text{Bi}_2\text{Fe}_4\text{O}_9$  and  $\text{Bi}_{36}\text{Fe}_{24}\text{O}_{57}$  at  $2\theta = 25.75^\circ$ ,  $30.33^\circ$ ,  $48.41^\circ$  and  $49.30^\circ$  and  $24.64^\circ$ ,  $30.31^\circ$ ,  $33.28^\circ$ ,  $42.07^\circ$ ,  $43.43^\circ$ ,  $54.29^\circ$ ,  $55.55^\circ$ , respectively. The difference in oxygen affinity of Fe and Bi ion was responsible for the generation of secondary impurity phases. Further, as we increased the calcination temperature to  $550\text{ }^\circ\text{C}$  and  $650\text{ }^\circ\text{C}$ , the sharpening of main diffraction peaks increased and intensity of secondary impurity phases decreased. In case of sample calcinated at  $650\text{ }^\circ\text{C}$ , miller indices, i.e., (012), (104), (110), (006), (202), (024), (116), (122), (214), (018) and (300) were found corresponding to the main diffraction peaks  $22.5$ ,  $31.78$ ,  $32.0$ ,  $38.96$ ,  $39.09$ ,  $46.05$ ,  $51.47$ ,  $51.73$ ,  $55.54$ ,  $55.59$  and  $55.87^\circ$  of  $\text{BiFeO}_3$  nanoparticles, which were accordingly with the JCPDS Card no. 86-1518 [29]. So from above discussion calcination temperature  $650\text{ }^\circ\text{C}$ , showing that more is the calcination temperature more will be the sharpening of main diffraction peaks with more will be the elimination of impurity phases [30, 31]. Now to check whether  $650\text{ }^\circ\text{C}$  temperature was the final calcination temperature for obtaining pure form of  $\text{BiFeO}_3$  nanoparticles, we also extend our study on more calcination



**Fig. 2** XRD analysis of  $\text{BiFeO}_3$  calcinated at **a**  $150\text{ }^\circ\text{C}$ , **b**  $450\text{ }^\circ\text{C}$ , **c**  $550\text{ }^\circ\text{C}$ , **d**  $650\text{ }^\circ\text{C}$ , **e**  $750\text{ }^\circ\text{C}$  and **f**  $850\text{ }^\circ\text{C}$



temperatures such as 750 °C and 850 °C. In case of 750 °C, impurity phases such as  $\text{Bi}_2\text{O}_3$ ,  $\text{Bi}_3\text{Fe}_4\text{O}_9$ ,  $\text{Bi}_2\text{Fe}_4\text{O}_4$  [32] and  $\text{Bi}_{36}\text{Fe}_{24}\text{O}_{57}$  [33] were found at  $2\theta = 14.79^\circ$  and  $32.99^\circ$ , respectively. On further increasing the calcination temperature to 850 °C, the sample lost its main diffraction peaks with more impurity phases at  $2\theta = 14.79, 28.99, 29.81, 33.80, 47.27$  and  $49.49^\circ$  for  $\text{Bi}_2\text{O}_3$ ,  $\text{Bi}_3\text{Fe}_4\text{O}_9$  [32] and  $\text{Bi}_2\text{Fe}_4\text{O}_4$  [33], respectively. So 650 °C temperature was the optimized calcinated temperature for obtaining pure form of  $\text{BiFeO}_3$  nanoparticles. Further using Scherrer's formula  $D = k\lambda/\beta \cos\theta$ , where  $\lambda$  is the wavelength,  $\beta$  is the corrected diffraction line full-width at half maximum,  $k$  is a constant (having a value of 0.94) and is Bragg's angle, average particle size was calculated for calcination temperature 150 °C, 450 °C, 550 °C and 650 °C and was found to be approximately 5.74 nm, 11.79 nm, 69.3 nm and 70.01 nm, respectively. The increase in particles size with increasing calcination temperature was due to the formation of cluster, particles collision [34] and sharpening of main diffraction peaks [35].

### VSM

Investigation regarding magnetic property of as-synthesized samples, i.e.,  $\text{BiFeO}_3$  nanoparticles using sucrose as chelating agent at different ranges of calcination temperature over a magnetic field  $\pm 1\text{ T}$  was carried out as demonstrated in Fig. 3. The value of saturation magnetization ( $M_s$ ) of sample calcinated at temperature 150 °C, 450 °C, 550 °C and 650 °C was found to be 0.6 emu/g, 5.6 emu/g, 2.5 emu/g and 0.4 emu/g, respectively. The main reason of showing magnetic properties by  $\text{BiFeO}_3$  nanoparticles was due to the existence of  $\text{Fe}^{3+}$  ions and excess of oxygen vacancies [32]. The decrease in  $M_s$  value from 450 °C to 650 °C is that some grains are unable to contribute in magnetization because they do not possess spontaneous magnetic moment at higher temperature and increase in bond length of Bi–Fe

bond and bond angles of Fe–O–Fe, Fe–O–Fe bonds [36, 37]. The low value of  $M_s$  at 150 °C was attributed to the little bit formation of Fe–O and O–Fe–O bonds, and higher value of  $M_s$  of calcination temperature 450 °C as compared to calcination temperature 150 °C was due to the complete appearance of the formation of Fe–O and O–Fe–O bonds [25] as also explained by FT-IR and XRD analysis earlier. So as pure form of  $\text{BiFeO}_3$  nanoparticles was obtained at calcination temperature 650 °C as explained by XRD earlier and exhibiting 0.4 emu/g of saturation magnetization ( $M_s$ ) by VSM, proved it as a potential material to be used as magnetically separable in numerous applications [38].

### TEM

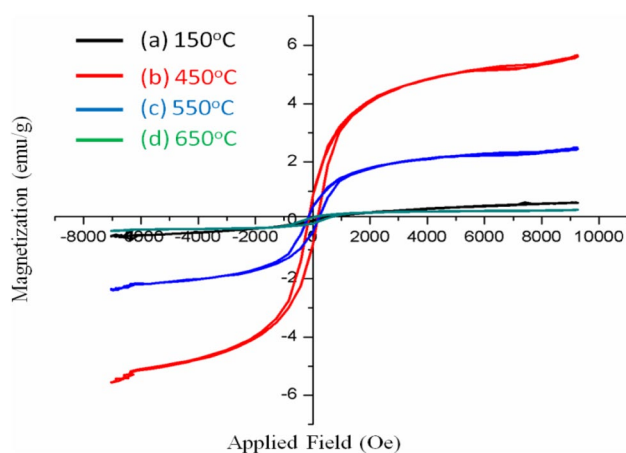
Study of particle size and morphology was explored by TEM analysis. The TEM analysis of  $\text{BiFeO}_3$  nanoparticles using sucrose as chelating agent at calcination temperature 150 °C and 650 °C has been done as exposed in Fig. 4. Grain particle size exhibited by this analysis was found to be large as compared to the average particle size by XRD analysis. The reason behind is that some grain contains sub-grains which were separated by low-angle grain boundaries [39].

### BET

The surface area of  $\text{BiFeO}_3$  nanoparticles using sucrose as chelating agent at different calcination temperature, i.e., 150 °C, 450 °C, 550 °C and 650 °C was found to be  $6.4\text{ m}^2/\text{g}$ ,  $2.1\text{ m}^2/\text{g}$ ,  $1.8\text{ m}^2/\text{g}$  and  $1.6\text{ m}^2/\text{g}$ , respectively. The decrease in surface area with increase in calcination temperature was attributed to the increase in particle size; results were in good agreement as explained by XRD and TEM analysis earlier [40].

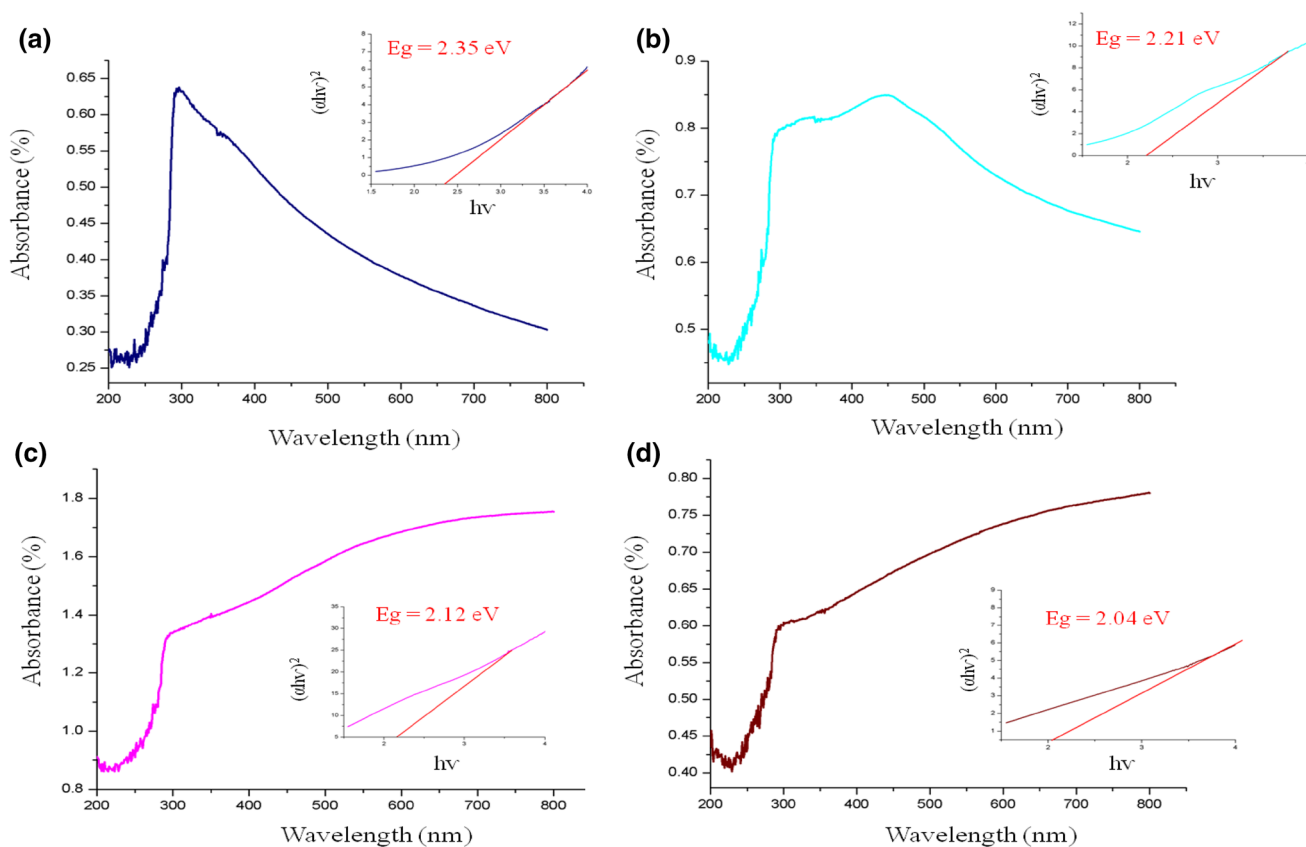
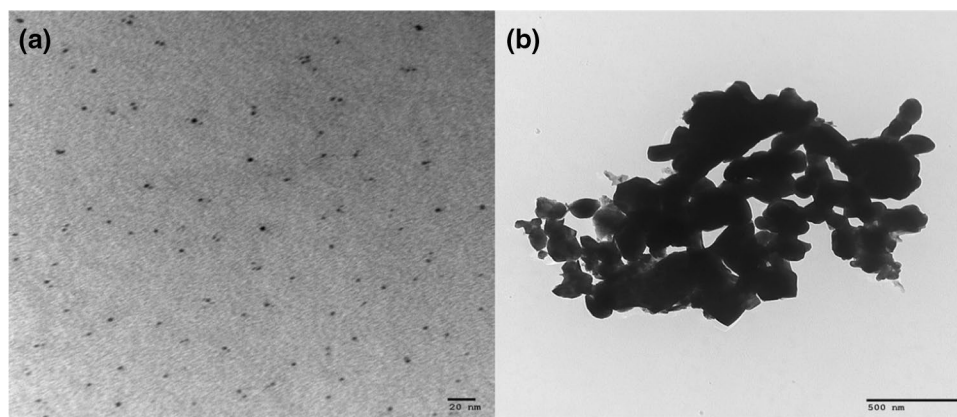
### UV–Vis analysis

UV–Vis analysis of as-synthesized samples using sucrose as a chelating agent prepared at different calcination temperature, i.e., 150 °C, 450 °C, 550 °C and 650 °C, was carried out as shown in Fig. 5. The nanoparticles showed a strong absorption in visible light, which is related to the band gap energy of the photocatalyst. Tauc's equation was used for the estimation of band gap,  $(\alpha h\nu)^n = B(h\nu - E_g)$ . Where  $\alpha$ ,  $h$ ,  $\nu$ ,  $E_g$  and  $B$  are the absorption coefficient, Plank constant, light frequency, band gap energy and a constant, respectively. For  $\text{BiFeO}_3$ ,  $n=2$ , which indicates the direct band gap. The band gap energy was calculated by extrapolating the linear portion of  $(\alpha h\nu)^2$  vs  $h\nu$  to the point  $\alpha=0$ . The value of band gap observed using above formula was found to be 2.35 eV, 2.21 eV, 2.12 eV and 2.04 eV for the sample prepared at 150 °C, 450 °C, 550 °C and 650 °C, respectively. The basic reason for the change in band gap at nanoscale is that when



**Fig. 3** VSM of  $\text{BiFeO}_3$  nanoparticles calcinated at **a** 150 °C, **b** 450 °C, **c** 550 °C, and **d** 650 °C

**Fig. 4** TEM analysis of  $\text{BiFeO}_3$  calcinated at **a** 150 °C and **b** 650 °C



**Fig. 5** UV-Vis spectra of  $\text{BiFeO}_3$  calcinated at **a** 150 °C, **b** 450 °C, **c** 550 °C, and **d** 650 °C

the size of particle reaches to nanoscale, number of overlapping of orbitals decreases and thickness of band becomes thinner. These will result into the increase in energy band gap between the valence and conduction band. This behavior of band gap is in good agreement with the previous reports for perovskite type nanomaterials [41]. Moreover, band gap also depends on the particle size of nanoparticles. As in our case average particles size increased with

increase in calcination temperature, i.e., 5.74 nm, 11.79 nm, 69.3 nm and 70.01 nm observed for  $\text{BiFeO}_3$  nanoparticles prepared at 150 °C, 450 °C, 550 °C and 650 °C, respectively, as discussed earlier by XRD analysis. The reason behind the decrease in band gap with increase in average particle size is the “quantum size effect” which leads to increase in  $E_g$  values with decrease in average particle size nanoparticles [42, 43]. So  $\text{BiFeO}_3$  nanoparticles prepared

at calcination temperature 650 °C exhibited least value of band gap energy, i.e., 2.04 eV which is in agreement with the previous literature [22, 44]. This proves that as-prepared catalyst is appropriate for acting as photocatalyst for the degradation of harmful compounds in the range of visible light. It has been observed that there is slightly a redshift in the absorption edges, i.e., 292.92 nm, 290.98 nm, 288.15 nm and 286.20 nm for the sample calcinated at 150 °C, 450 °C, 550 °C and 650 °C, respectively. This observation demonstrated that redshift with increasing calcination temperature is an indicative of decrease in band gap with increase in crystalline size (as shown in Fig. 5). These results are in well agreement with the previous reports [45].

## Catalytic activity

### Photocatalytic activity

The catalytic activity of as-synthesized BiFeO<sub>3</sub> nanoparticles has been evaluated for photocatalytic degradation of RhB and tartrazine in aqueous media. No additives have been added in the reaction of both dyes. Various parameters such as effect of BiFeO<sub>3</sub> prepared by different chelating agents at calcination temperature of 150 °C, effect of BiFeO<sub>3</sub> prepared by different chelating agents at calcination temperature of 650 °C, effect of pH, effect of different calcination temperature, dose of catalytic amount, optimization of reaction condition, optimization of dye solution (ml), optimization of dye concentration (ppm), optimization of time and recyclability were investigated. The degradation efficiency was evaluated by using the formula:

$$\% \text{Degradation} = (C_0 - C_t / C_0) \times 100 \quad (1)$$

where  $C_0$  is the initial concentration of RhB and tartrazine and  $C_t$  is the concentration at time  $t$ .

### Effect of BiFeO<sub>3</sub> prepared by different chelating agents at calcination temperature of 150 °C

To find out the better chelating agent (i.e. sucrose, tartaric acid, urea and citric acid) for the synthesis of BiFeO<sub>3</sub> nanoparticles and their effects on the degradation of dyes were checked. Effect of BiFeO<sub>3</sub> prepared by these different chelating agents and calcinated at initial temperature, i.e., 150 °C and on percentage degradation of RhB and tartrazine was explored. Study was also carried out by BiFeO<sub>3</sub> prepared without using any chelating agent. Data as illustrated in Table 1 (Entry 1–5) demonstrate that better results were given by BiFeO<sub>3</sub> prepared by using sucrose as a chelating agent.

### Effect of BiFeO<sub>3</sub> prepared by different chelating agents at calcination temperature of 650 °C

Further we also continue our investigation on the different types of catalyst prepared at calcination temperature 650 °C. The same reaction conditions were used for the degradation of RhB and tartrazine as given above. The effect on % degradation was investigated by all types of catalysts prepared by different chelating agents as shown in Table 1 (Entry 6–10). From above discussion, it was clear that better results were given by the catalysts when prepared at 650 °C as compared to prepared at 150 °C. This shows that as we increased the calcination temperature, the purity of the BiFeO<sub>3</sub> nanoparticles enhanced and band gap decreases (as shown in Fig. 5) which was responsible for fast degradation process. These results were in good agreement as demonstrated by XRD analysis. Further, observation shows that best catalyst for degradation was BiFeO<sub>3</sub> nanoparticles prepared by chelating agent sucrose. It shows better catalytic activity among all the catalysts prepared at calcination temperature of 650 °C (citric acid, tartaric acid and urea as chelating agent). The reason for better catalytic activity was due to the value of band

**Table 1** Effect on % degradation by catalyst prepared at 150°C

Entry	Catalyst	Chelating agent	Calcination Temp.	Amount (mg)	% Degradation (RhB)	% Degradation (Tartrazine)
1	BiFeO <sub>3</sub>	–	150 °C	10	0.33	24.37
2	BiFeO <sub>3</sub>	Sucrose	150 °C	10	70.36	42.13
3	BiFeO <sub>3</sub>	Citric acid	150 °C	10	0.60	24.84
4	BiFeO <sub>3</sub>	Tartaric acid	150 °C	10	7.01	33.89
5	BiFeO <sub>3</sub>	Urea	150 °C	10	3.23	25.15
6	BiFeO <sub>3</sub>	–	650 °C	10	14.86	25.47
7	BiFeO <sub>3</sub>	Sucrose	650 °C	10	82.45	70.44
8	BiFeO <sub>3</sub>	Citric acid	650 °C	10	68.14	53.14
9	BiFeO <sub>3</sub>	Tartaric acid	650 °C	10	68.90	61.16
10	BiFeO <sub>3</sub>	Urea	650 °C	10	71.37	65.40

Reaction conditions: 10 ml (10 ppm dye sol), pH(RhB; 6.84, tartrazine; 7.2) (30 min stirring in dark, 60 min stirring under sunlight)



gap energy which plays an important role in the degradation process. It has been found that the values of band gap energies for BiFeO<sub>3</sub> nanoparticles prepared by using different chelating agent citric acid, tartaric acid, urea and sucrose were found to be 2.25 eV, 2.20 eV, 2.17 eV and 2.04 eV with % degradation of RhB (68.14%, 68.90%, 71.37% and 82.45%) and tartrazine (53.14%, 61.16%, 65.40% and 70.44%), respectively. So it was observed that the value of percentage degradation of both dyes increased with decrease in the band gap. The reason for increase in photocatalytic activity with decrease in band gap was attributed to the production of inter-band or heterojunction which decreases the electron-hole recombination [16, 46]. So, finally BiFeO<sub>3</sub> prepared by sucrose as chelating agent with calcination at 650 °C was the optimized catalyst for the reaction.

### Optimization of pH

Since the industrial waste consists of wide range of pH values, so it is necessary to check the catalytic activity of

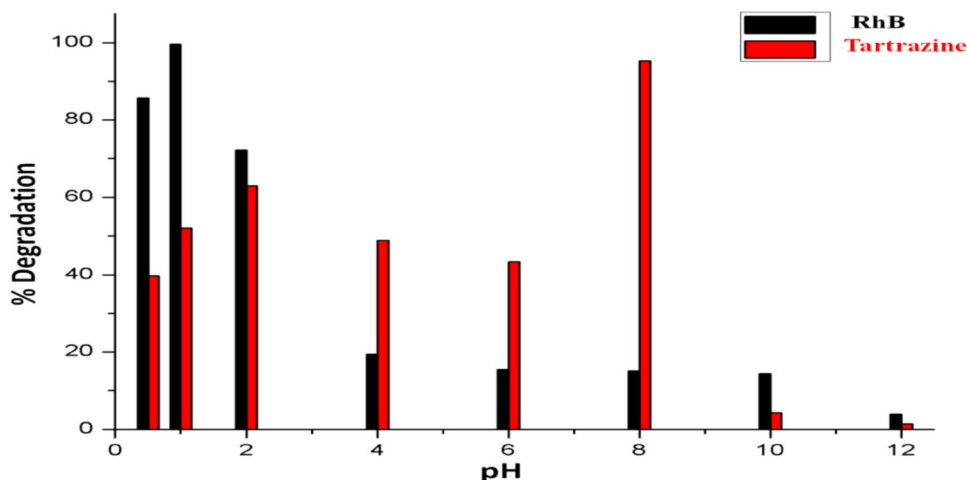
**Table 2** Effect of pH on % degradation<sup>a</sup>

Entry	pH	Amount (mg)	% Degradation (RhB)	% Degradation (tartrazine)
1	0.5	10	85.71	39.76
2	1	10	99.62	52.03
3	2	10	72.21	62.95
4	4	10	19.42	48.83
5	6	10	15.54	43.43
6	8	10	15.10	95.40
7	10	10	14.46	4.20
8	12	10	3.90	1.4

Reaction conditions: 10 ml (10 ppm dye sol), BiFeO<sub>3</sub> (10 mg), 30 min stirring in dark, 60 min stirring under sunlight

as-synthesized catalyst at different range of pH. The pH factor affects the surface charge properties of the catalyst and the formation of ionic species in the solution [2]. So it is the one of the most significant parameters which influences the % degradation of dyes. For this purpose, dye solution of RhB and tartrazine were prepared at different pH, i.e., 0.5, 1, 2, 4, 6, 8, 10 and 12. The pH values of dye solution were adjusted by using HCl and NaOH solution of 1 N each as demonstrated in Table 2 and Fig. 6. Further the point of zero charge of as-synthesized BiFeO<sub>3</sub> nanoparticles was calculated by using pH drift method [47] and found to be 7.006. In case of RhB (cationic dye), the catalyst shows maximum degradation efficacy (99.62%) in acidic medium, i.e., at pH 1. The reason behind the higher % degradation in acidic medium was due to the fact that when pH < 4, there was a shifting of carboxylic group of RhB to the acidic form. Because of the equilibrium, the existence of carboxylic ions in the medium adsorbed on the surface and then the equilibrium shifted to balance the adsorbed species. This process continues to whole degradation. With lower % degradation at higher pH equal or greater than 4, there was a formation of zwitterion of RhB because of the ionization of carboxylic acid group. Force of attraction between the carboxyl and the xanthenes causes the demerization of zwitterion of RhB in water. This brings the increase in the size of molecule and decrease in density of charge due to the interaction between the two monomers which further inhibited the removal [2]. In case of tartrazine (anionic dye) maximum degradation efficacy (95.40%) in alkaline medium, i.e., at pH 8 was observed. Rate of degradation in basic medium was higher than in acidic medium. The reason behind it might be more availability of hydroxyl ion which generates more number of OH<sup>•</sup> radicals, responsible for degradation process [48].

**Fig. 6** Variation of % degradation with pH, reaction conditions: 10 ml (10 ppm dye sol), BiFeO<sub>3</sub> (10 mg), 30 min stirring in dark, 60 min stirring under sunlight



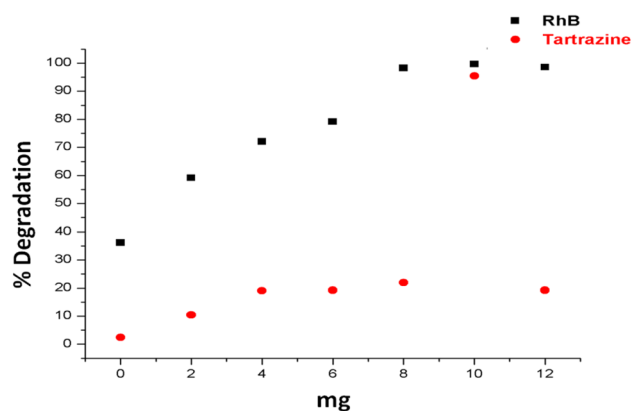
### Effect of calcination temperature

After deciding the better  $\text{BiFeO}_3$  among different chelating agents, i.e.,  $\text{BiFeO}_3$  prepared by sucrose as chelating agent with calcination at  $650^\circ\text{C}$ , effect of pH, i.e., 1 for RhB and 8 for tartrazine of 10 ppm of dye solution, next, we elaborated our study on the  $\text{BiFeO}_3$  prepared by using sucrose as chelating agent and calcinated at different ranges of temperature such as  $150^\circ\text{C}$ ,  $450^\circ\text{C}$ ,  $550^\circ\text{C}$ ,  $650^\circ\text{C}$ ,  $750^\circ\text{C}$  and  $850^\circ\text{C}$ . RhB dye showed % degradation of 95.03, 98.75, 99.50, 99.62, 99.00, 87.45, and tartrazine showed % degradation of 4.97, 5.42, 74.88, 95.40, 68.77, 62.21 by  $\text{BiFeO}_3$  nanoparticles prepared at  $150^\circ\text{C}$ ,  $450^\circ\text{C}$ ,  $550^\circ\text{C}$ ,  $650^\circ\text{C}$ ,  $750^\circ\text{C}$  and  $850^\circ\text{C}$ , respectively. Here we observed that as we increased the calcination temperature, i.e., from 150 to  $650^\circ\text{C}$ , % degradation of both dyes increased, but further increasing temperature from 750 to  $850^\circ\text{C}$ , % degradation in both cases decreased. The main reason for this observation is that as we increased the calcination temperature, the purity  $\text{BiFeO}_3$  nanoparticles increased and maximum purity is obtained at  $650^\circ\text{C}$ . Further at higher temperature, i.e., at  $750^\circ\text{C}$  and  $850^\circ\text{C}$ , the purity decreases by the formation of new impurity phases as it was also cleared by XRD study. So,  $\text{BiFeO}_3$  nanoparticles prepared at calcination temperature  $650^\circ\text{C}$  show maximum catalytic activity for the degradation of both dyes as depicted in Fig. 7.

### Dose of catalyst

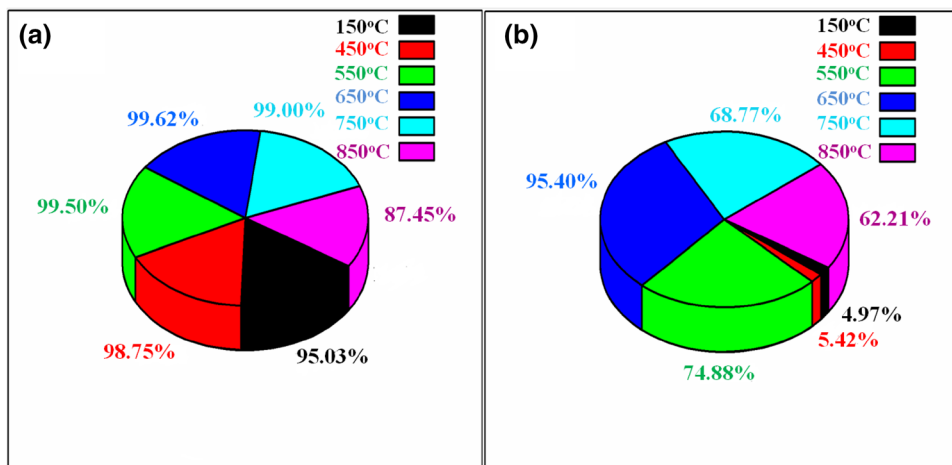
Experiments were carried out by using different amounts of the catalyst, i.e., 0, 2, 4, 6, 8, 10 and 12 mg keeping concentration of both dyes 10 ppm, dye solution 10 ml each, pH (1 for RhB, 8 for tartrazine) under sunlight, and values of % degradation were found to be 36.14, 59.13, 72.04, 79.13, 98.26, 99.62 and 98.54 for RhB and 2.48, 10.40, 19.00, 19.23, 21.94, 95.40 and 19.00 for tartrazine, respectively.

It was found that % degradation of both dyes first increases and shows maximum efficiency at 10 mg/10 ml of dye solution beyond which it shows reduction. The increase in % degradation with increasing catalytic amount may be attributed due to increase in catalytic active site available on the catalyst surface for the reaction, which in turn increased the hydroxyl and superoxide radicals that were essential for the photocatalysis process [49]. The reduction in % degradation with increasing the catalytic amount beyond 10 mg/10 ml dye solution is due to the scattering of light and decrease in penetration of light through the dye solution. Further, deactivation of the active molecules by the collision with the ground state molecules causes the decrease in the efficiency of the catalytic activity of the catalyst, which results in reduction in % degradation of dyes [50, 51] as shown in Fig. 8. So from above, it was observed that 10 mg amount of the catalyst is the appropriate amount which shows maximum degradation, i.e., 99.62% and 95.40% for RhB and tartrazine dyes, respectively.



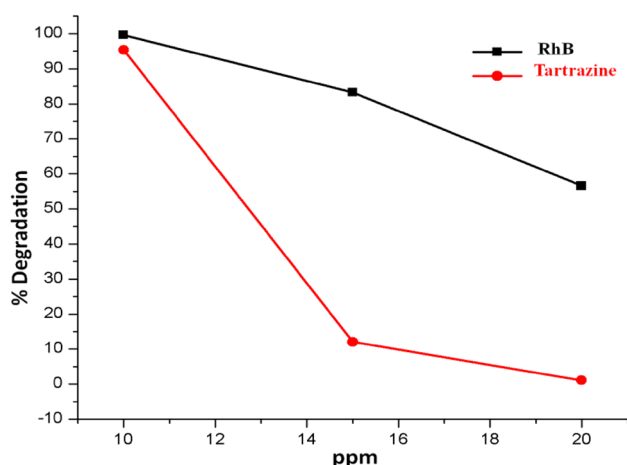
**Fig. 8** Effect of dose of catalyst on % degradation, Reaction conditions: 10 ml (10 ppm dye sol), pH (1 for RhB, 8 for tartrazine),  $\text{BiFeO}_3$  (mg), 30 min stirring in dark, 60 min stirring under sunlight

**Fig. 7** Effect of calcination temperature on % degradation, **a** RhB, **b** tartrazine, reaction conditions: 10 ml (10 ppm dye sol), pH (1 for RhB, 8 for tartrazine),  $\text{BiFeO}_3$  (10 mg), 30 min stirring in dark, 60 min stirring under sunlight



### Effect of concentration of dye

The effect concentration of dyes RhB and tartrazine was studied by changing the concentration, i.e., 10, 15 and 20 ppm, keeping the BiFeO<sub>3</sub> (10 mg/10 ml) constant. The % degradation of RhB and tartrazine was found to be decreased with increase in dye concentration. Since the availability of the catalytic active sites for the reaction is critical for the degradation to take place. Number of factors is responsible for decrease in % degradation of dyes. As we increased the dye concentration, more and more number of molecules of dye gets adsorbed on the surface of catalyst and requirement of reactive species (OH<sup>•</sup> and O<sub>2</sub><sup>•−</sup>) for the degradation of dye also increases. Since at a particular light intensity, catalytic amount and irradiation time, the formation of reactive species is also constant (which is responsible for dye degradation) [52, 53]. As we increase the dye concentration by keeping the catalytic amount constant, this causes the decrease in the active sites of the catalyst. Further increase the dye concentration, the color of the solution becomes more intense, which results in decrease in the path length of the entering photons into the solution. And only fewer photons reach the surface of catalyst for the formation of hydroxyl and superoxide radical gets decreased [50, 51]. RhB shows % degradation of 99.62, 83.23, 56.55, and tartrazine shows % degradation of 95.40, 12.03, 1.05 at 10 ppm, 15 ppm and 20 ppm dye concentration, respectively. Our observation is in good agreement with the reported literature as shown in Fig. 9. So, 10 ppm dye concentration was found to be optimized amount to carry out the reaction.



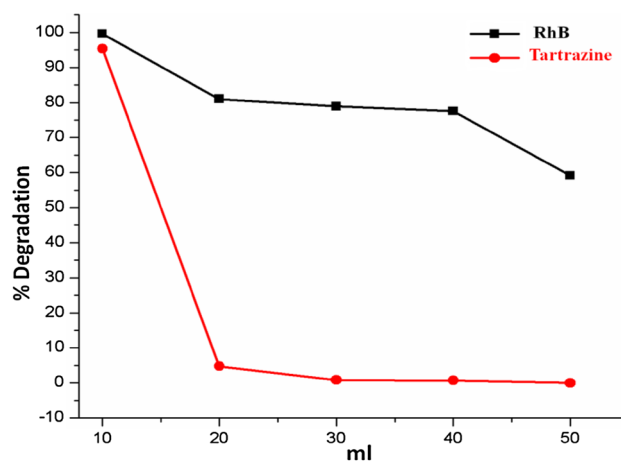
**Fig. 9** Effect of dye concentration on % degradation, reaction conditions: 10 ml (ppm dye sol), pH (1 for RhB, 8 for tartrazine), BiFeO<sub>3</sub> (10 mg), 30 min stirring in dark, 60 min stirring under sunlight

### Effect of amount of dye solution

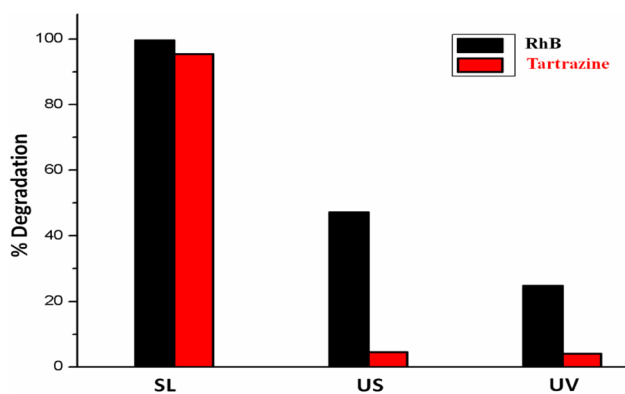
After optimization of the concentration of dye, i.e., 10 ppm, our next step was to investigate the effect of different amount (ml) of dye solution. For this investigation, different amount of dye solution 10 ml, 20 ml, 30 ml, 40 ml and 50 ml of pH (1 for RhB, 8 for tartrazine) was taken by fixing BiFeO<sub>3</sub> nanoparticles (10 mg) and under sunlight. The % degradation was decreased as we increased the amount of dye solution (ml). The % degradation for RhB observed were 99.62, 80.99, 78.88, 77.51, 59.13 and for tartrazine, 95.40, 4.75, 0.8, 0.7, 0.008 for 10 ml, 20 ml, 30 ml, 40 ml and 50 ml, respectively. As we increased the amount of dye solution, more number of molecules of dye gets adsorbed on the surface of catalyst which in turn decreases the availability of active sites of the catalyst for the reaction and results into decrease in the % degradation of the dyes [5, 54]. It was found that maximum efficiency was shown by catalyst in 10 ml of both dye solutions as illustrated in Fig. 10. So, finally 10 ml amount was selected as optimized amount for both dye solutions.

### Optimization of reaction condition

The photodegradation of RhB and tartrazine was also carried out under different reaction conditions to find out the appropriate condition to do the experiment. For this purpose, the reaction was carried out using optimum conditions, i.e., amount of catalyst of BiFeO<sub>3</sub> nanoparticles (10 mg), concentration of dye solution (10 ppm), amount of dye solution (10 ml) and pH (1 for RhB, 8 for tartrazine) under sunlight (SL), ultra-sonication (US) and ultra-violet (UV) as shown in Fig. 11. Better results were found under sunlight irradiation. Although only 5% optimum energy of sunlight is for photodegradation of industrial



**Fig. 10** Effect of amount of dye solution on % degradation, reaction conditions: ml (10 ppm dye sol), pH (1 for RhB, 8 for tartrazine), BiFeO<sub>3</sub> (10 mg), 30 min stirring in dark, 60 min stirring under sunlight



**Fig. 11** Effect of different reaction conditions on % degradation, reaction conditions: 10 ml (10 ppm dye sol), pH (1 for RhB, 8 for tartrazine), BiFeO<sub>3</sub> (10 mg), 30 min stirring in dark, 60 min stirring (under Sunlight SL, Ultra-sonication (US) and Ultra-violet (UV))

pollutants, it is safe and cost-effective. Both UV light source and Ultra-sonication are costly and dangerous to health [5], which renders our catalytic systems environmental friendly as the ultimate source of energy is sun. The high activity in sunlight as compared to UV source clearly indicates that perovskite structure materials exhibit better catalytic activity under visible light due to its narrow band gap energies (2.04 eV) [2] as in our case. The results are in great agreement previous findings that BiFeO<sub>3</sub> nanoparticles can effectively utilize visible

light for the degradation of organic compounds in aqueous media [31, 55]. So reaction under sunlight irradiation was the appropriate reaction condition to do the experiment.

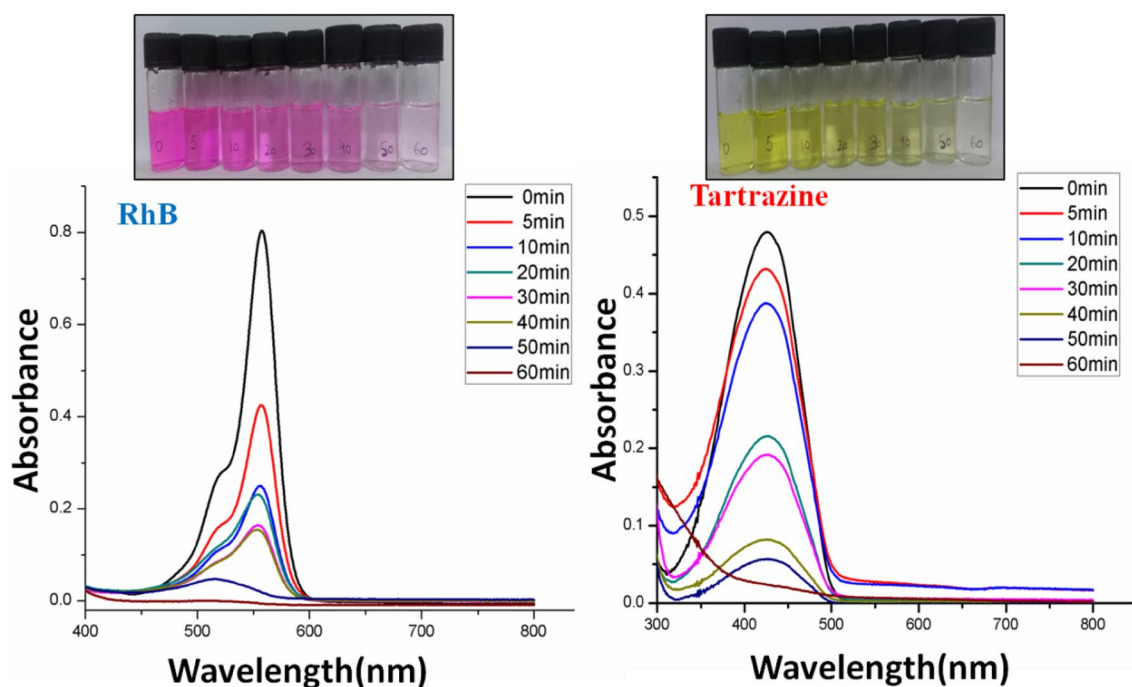
### Effect of stirring time on degradation

After analysis of numerous factors, further we investigated the effect of stirring time on the photoassisted degradation of RhB and tartrazine. Figure 12 depicts that photodegradation of both dyes using optimized conditions as a function of stirring time under solar light irradiations. The intensity of main absorption peak (557 nm for RhB and 425 nm for tartrazine) decreased with irradiation time which indicates the decrease in the concentration of dye, thus dye being gradually degraded. The results demonstrated that the high activity of the as-prepared catalyst caused the degradation of RhB and tartrazine dyes [11].

### Kinetic study of photodegradation

Photocatalytic degradation rate of most organic compounds follows pseudo-first-order kinetics. Photodegradation rate of organic compounds on the surface of semiconductor is described by the Langmuir–Hinshelwood model [56].

$$R = \frac{dC}{dt} = \frac{k_r KC}{1 + KC} \quad (2)$$



**Fig. 12** Effect of stirring time on % degradation, reaction conditions: 10 ml (10 ppm dye sol), pH (1 for RhB, 8 for tartrazine), BiFeO<sub>3</sub> (10 mg), 30 min stirring in dark, (0–60 min) stirring under sunlight

where  $k_r$  = reaction rate constant,  $K$  = adsorption coefficient of the reaction,  $C$  = reactant concentration.

The effect of light intensity is also included in  $k_r$ , and  $K$  expresses the equilibrium constant for adsorption–desorption phenomenon on interface between surface monolayer and bulk solution. Integration of (Eq. 1) gives the following equation.

$$\ln(C_0/C) + K(C_0 - C) = k_r Kt \quad (3)$$

When the initial concentration  $C_0$  is small, (Eq. 3) becomes (Eq. 4), which reveals a pseudo-first-order reaction kinetics.

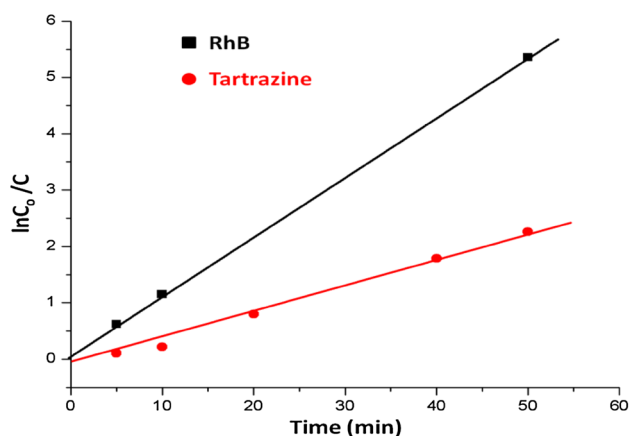
$$\ln(C_0/C) = k_r Kt = kt \quad (4)$$

For pseudo-first order reaction half life  $t_{1/2} = 0.693/k$ , where  $k$  is the pseudo-first-order reaction rate constant in  $\text{min}^{-1}$ . Figure 13 shows the plot of  $\ln(C_0/C)$  versus time of two dyes.

Rate constant ( $k$ ) in each case, i.e., rhodamine and tartrazine, is calculated from the slopes of the respective curves [57, 58] as in Fig. 13. The value of rate constant and half life time  $t_{1/2}$  is tabulated in Table 3.

### Stability and reusability of the catalyst

The estimation of stability and reusability of the as-synthesized catalyst is an important parameter for practical point of view for further application. For the determination of this, photodegradation experiment was repeated for five cycles. In case of each cycle, the catalyst was separated from the reaction mixture by using an external magnet. Then the collected sample was used in consecutive cycles for degradation as shown in Fig. 14. The minor change in performance of catalyst with each cycle might be due to the reduction in catalytic active sites [59].



**Fig. 13** Plot of photodegradation rate of rhodamine B and tartrazine on  $\text{BiFeO}_3$  w.r.t. irradiation time under sunlight

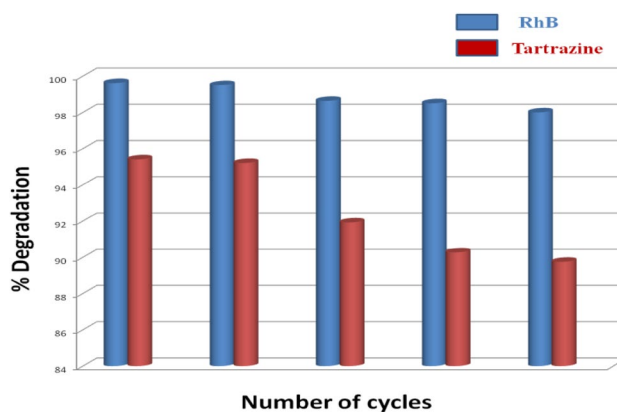
**Table 3** Kinetic data of both dyes using  $\text{BiFeO}_3$  nanoparticles as photocatalyst

S. No.	Dye	$K (\text{min}^{-1})$	$t_{1/2} (\text{min})$
1	Rh B	0.37	1.86
2	Tartrazine	0.05	13.07

### Adsorption vs photodegradation

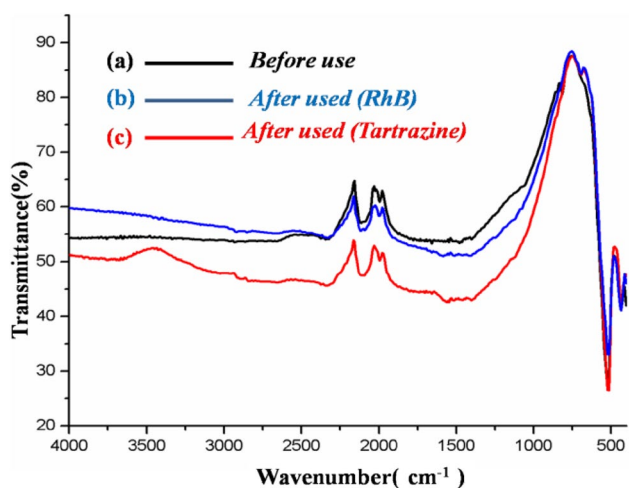
The decolorization of dye solution may be due to either adsorption of dye on the surface of the catalyst or adsorption of dye followed by its degradation by photoexcited electrons. Thus, to establish the phenomenon responsible for decolorization of dye and stability of the catalyst, the FT-IR spectra of the catalyst before and after use (in both cases of dyes) were recorded in Fig. 15. The above confirmation is verified by Fig. 15 which shows that decolorization of dye is resulting from its photodegradation because if only adsorption had been occurring, the FT-IR of catalyst taken after the photocatalytic reaction should have shown peaks due to the presence of dye also. But the spectra of fresh catalyst and after use have come out to be identical and also, there is not even a single peak indicating the presence of dye on the surface of catalyst, thus confirming the process of photodegradation of dye and also showed the stability of the catalyst after being reused.

Further XRD of the catalyst after use (in both cases of dyes) was carried out as shown in Fig. 16. It has been observed that the XRD of the catalyst after used in both cases of dyes consist of the same main diffraction peaks as appeared in the catalyst before use. This shows that the structure of the catalyst did not change or we can say that the catalyst showed its stability after being used.



**Fig. 14** Recyclability of the as-prepared catalyst  $\text{BiFeO}_3$ , Reaction conditions: 10 ml (10 ppm dye sol), pH (1 for RhB, 8 for tartrazine),  $\text{BiFeO}_3$  (10 mg), 30 min stirring in dark, 60 min stirring under sunlight





**Fig. 15** FTIR of the catalyst **a** Before use, **b** after use in case of RhB, **c** after use in case of tartrazine

Further the color of the catalyst before and after use was also checked in both cases. It has been observed that there was no change in color observed as depicted in Fig. 17. This study demonstrated that RhB and tartrazine dyes degraded completely because there were no RhB and tartrazine dyes found on the surface of as-synthesized catalyst.

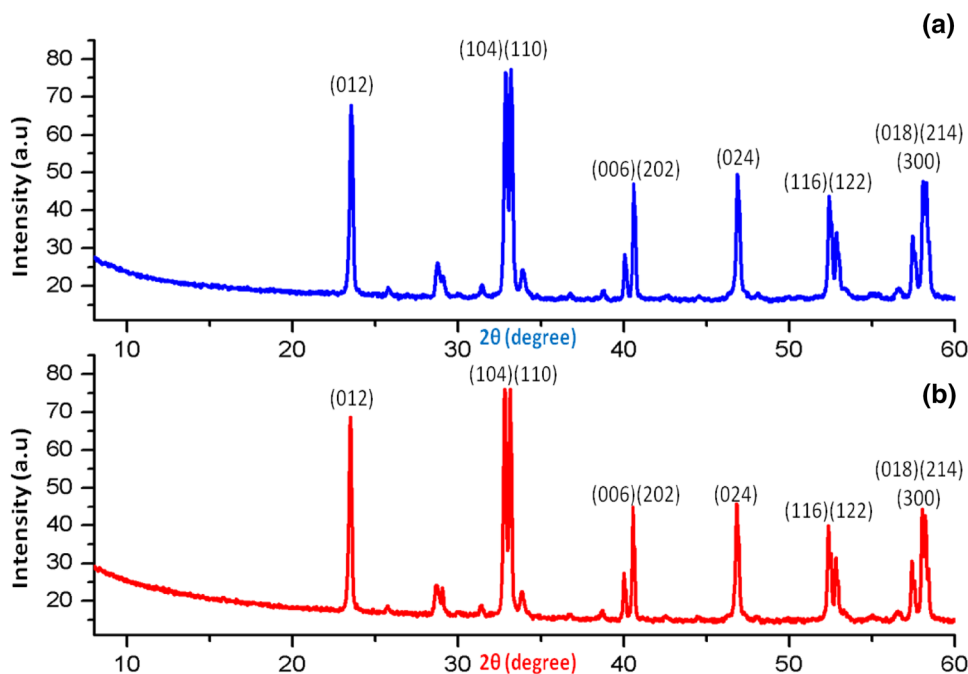
## Mechanism

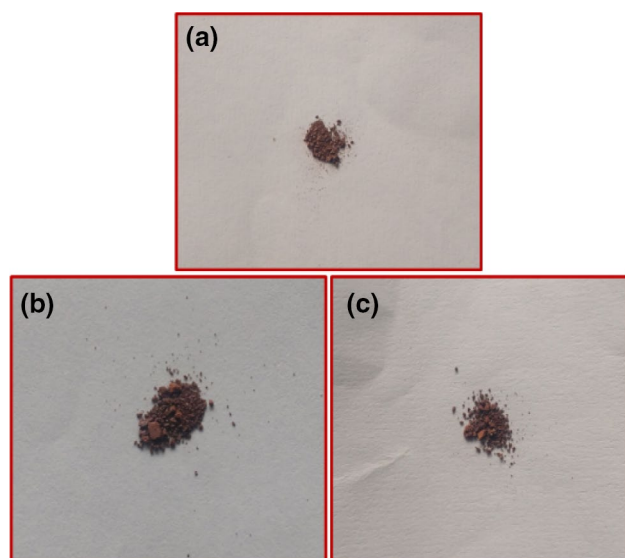
The proposed mechanism of the photodegradation of the dyes was also investigated. Under the sunlight irradiation, excitation of BiFeO<sub>3</sub> nanoparticles starts; the photon of

energy equal or greater than band gap causes the promotion of electrons ( $e^-$ ) from the valance band (VB) to conduction band (CB) of the photocatalyst leaving behind photogenerated hole ( $h^+$ ). Both species undergo redox reaction with the adsorbed species on the surface of the catalyst. Generation of hydroxyl ion and superoxide ion was done by the reaction of  $h^+$  with the surface bound water and reaction of  $e^-$  with oxygen, respectively, as illustrated in Scheme 2 [49];

The generation of active species such as  $\cdot OH$ ,  $h^+$  and  $\cdot O_2^-$  was also verified experimentally. The verification of hydroxyl radical ( $\cdot OH$ ), holes ( $h^+$ ) and superoxide radical ( $\cdot O_2^-$ ) was carried out by using 2-propanol(IPA), disodium EDTA, and 1,4-benzoquinone(BQ) as scavengers [60]. In the absence of scavengers, the degradation of RhB and tartrazine was found to be 99.62% and 95.40% in 60 min, respectively. But when IPA, EDTA and BQ were added, the degradation of RhB was decreased to 81.5%, 39.07%, 16.03%, respectively, and for tartrazine decreased to 70.02%, 43.59%, 30.51%, respectively. This confirmed that the scavengers consumed the active species generated during photocatalysis caused by BiFeO<sub>3</sub> nanoparticles. Since  $h^+$  and  $\cdot OH$  play an important role in the photocatalytic reaction, here  $h^+$  acted more  $\cdot OH$  in both cases. In photocatalytic system  $\cdot OH$  and  $\cdot O_2^-$  are produced by the reaction of  $e^-$  and  $h^+$  with the O<sub>2</sub> and H<sub>2</sub>O [60, 61]. Further the degradation extent was reduced with addition of BQ in both cases confirmed that  $\cdot O_2^-$  was formed and consumed in the reaction [62, 63]. The generation of  $\cdot OH$  was also caused by  $\cdot O_2^-$  by the series of chemical reaction. So we can say that the degradation process was caused the  $\cdot OH$  and  $h^+$ .

**Fig. 16** XRD of the catalyst after used in repeating cycles **a** in case of RhB, **b** in case of tartrazine





**Fig. 17** Color of the catalyst **a** Before use, **b** after use in case of RhB, **c** after use in case of tartrazine

Further the values of  $E_{CB}$  (conduction band potential) and  $E_{VB}$  (valence band potential) were calculated by using formula and were found to be 2.79 eV and 0.75 eV, respectively, as shown in Scheme 3;

$$E_{CB} = X - E_C - 1/2E_g$$

$$E_{VB} = E_{CB} + E_g,$$

where  $X$  is the absolute electronegativity denoted by geometric mean of absolute electronegativity of the constituent

atoms,  $E_C$  is the energy of free electrons of the hydrogen scale (4.5 eV) and  $E_g$  is the band gap value [64]. It has been observed that redox potential of  $\cdot\text{OH}/\text{OH}$  is 1.99 eV which is less positive than  $E_{VB}$  (2.79 eV) of  $\text{BiFeO}_3$  nanoparticles. This observation also confirmed the presence and responsibility of  $\cdot\text{OH}$  for degradation process [65].

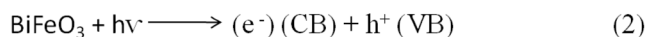
### FT-IR and mass analysis of products after degradation

#### FT-IR

The surface modification analysis of RhB dye before and after degradation has been explored. It has been observed that RhB dye solution before degradation shows an absorption band near  $3272\text{ cm}^{-1}$  was attributed to the stretching vibration of  $-\text{COOH}$  bonds and peaks related to  $-\text{C}=\text{C}-$ ,  $-\text{C}=\text{O}$ ,  $\text{Ar}-\text{N}-$ ,  $-\text{C}-\text{O}-\text{C}-$ ,  $-\text{C}-\text{H}$  and  $-\text{C}=\text{N}$  at  $1488\text{ cm}^{-1}$ ,  $1418\text{ cm}^{-1}$ ,  $1134\text{ cm}^{-1}$ ,  $1008\text{ cm}^{-1}$ ,  $983\text{ cm}^{-1}$  and  $487\text{ cm}^{-1}$  of aromatic ring system, respectively. When dye has undergone degradation after 60 min, the blueshift of  $-\text{COOH}$  bond was observed which results from the change in conjugate structure of RhB and intensity of peak corresponding above-mentioned groups totally disappeared indicates that large conjugated chromophore structure was totally damaged yielding smaller organic molecules as well as  $\text{Ar}-\text{N}(\text{C}_2\text{H}_5)_2$  bond and the ether bond ( $-\text{C}-\text{O}-\text{C}-$ ) in rhodamine B had been broken [66] as exposed in Fig. 18. In case of tartrazine before degradation the stretching vibration peak of chromophore ( $-\text{N}=\text{N}-$ ) was found at  $1557\text{ cm}^{-1}$ . After degradation this peak was not found. This clearly indicate that azo group

#### Scheme 2 Mechanism of degradation of dyes

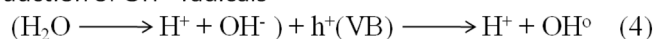
Step 1 Irradiation of  $\text{BiFeO}_3$  under sunlight, cause the formation of electron hole pairs



Step 2 Reduction of oxygen



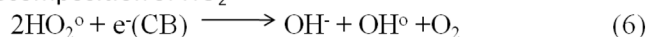
Step 3 Production of  $\text{OH}^\circ$  radicals



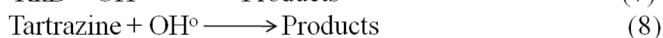
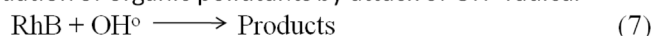
Step 4 Neutralization of  $\text{O}_2^{\cdot-}$  by photons

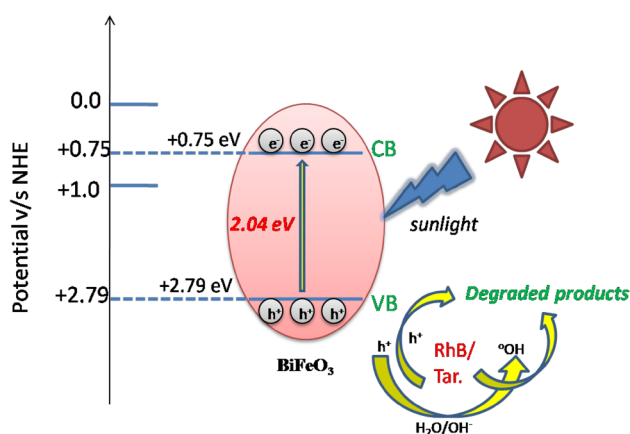


Step 5 Decomposition of  $\text{HO}_2^\circ$



Step 6 Oxidation of organic pollutants by attack of  $\text{OH}^\circ$  radical





**Scheme 3** Z-scheme diagram for BiFeO<sub>3</sub> nanoparticles system

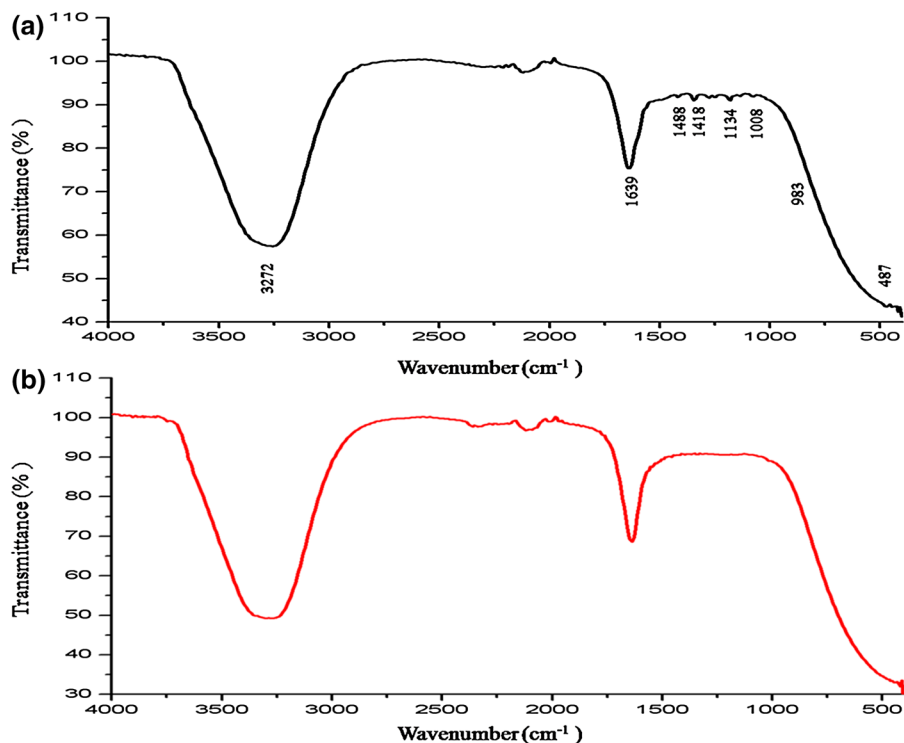
(-N=N-) was degraded from the sample. This observation further concluded that mechanism of discoloring of tartrazine occurred through degradation instead of adsorption [7, 67] as shown in Fig. 19.

### Mass analysis

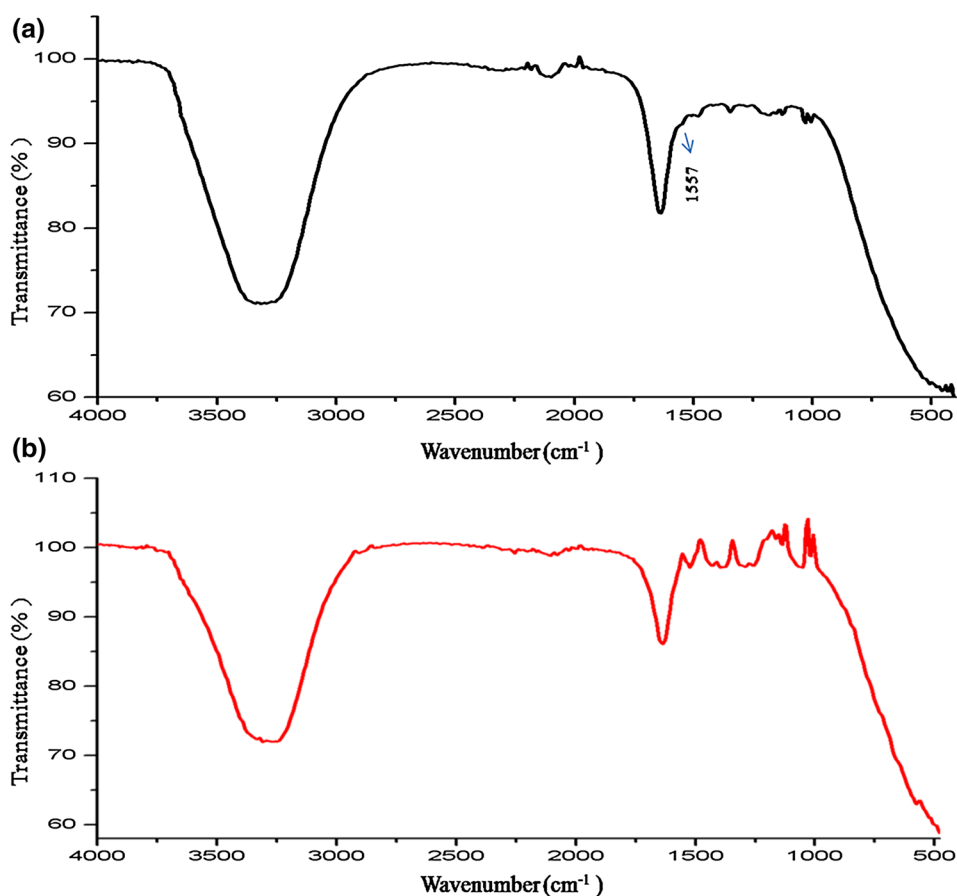
RhB has formula C<sub>28</sub>H<sub>31</sub>ClN<sub>2</sub>O<sub>3</sub>, in aqueous phase; it showed a molecular ion peak  $m/z$  at 443.16, in mass

spectrum of RhB before degradation because Cl<sup>-</sup> ion dissociates when it was dissolved in water Fig. 20a. In mass spectrum of RhB after degradation no peak corresponding to molecular ion was found which indicated that dye was degraded. The other peaks were observed corresponding to the degraded products of the dye. The  $m/z$  peaks obtained at 415 nm, 387 nm, 359 nm, 244 nm, 230 nm, 166 nm and 188 nm were attributed to the fragmented ions and were well matched with earlier reports [68–70] as depicted in Fig. 20b. Addition to these peaks, numerous peaks of insignificant intensity were also present in the spectrum which indicated that most of the RhB molecules have been mineralized. In case of tartrazine molecular ion peak found at  $m/z = 534$  in mass spectrum of dye before degradation was not found in mass spectrum of dye after degradation at same position, confirmed that tartrazine has undergone degradation as shown in Fig. 21. The  $m/z$  values of fragmented ions were observed at 240 nm, 172 nm and 157 nm which were in accordance with the degradation pathways reported in the literature [71, 72]. Further the structure of fragmented ions is free from -N=N- group, showing that dye has been broken into small ions or fragments. This observation is also in well agreement with the FT-IR analysis of tartrazine shown in Fig. 18b before. So from above discussion, it is clear that dye after degradation broken into small ions or intermediates which are lesser harmful than the respective dyes.

**Fig. 18** Comparison study of FT-IR of RhB **a** Before degradation, and **b** after degradation



**Fig. 19** Comparison study of FT-IR of tartrazine **a** Before degradation, and **b** after degradation



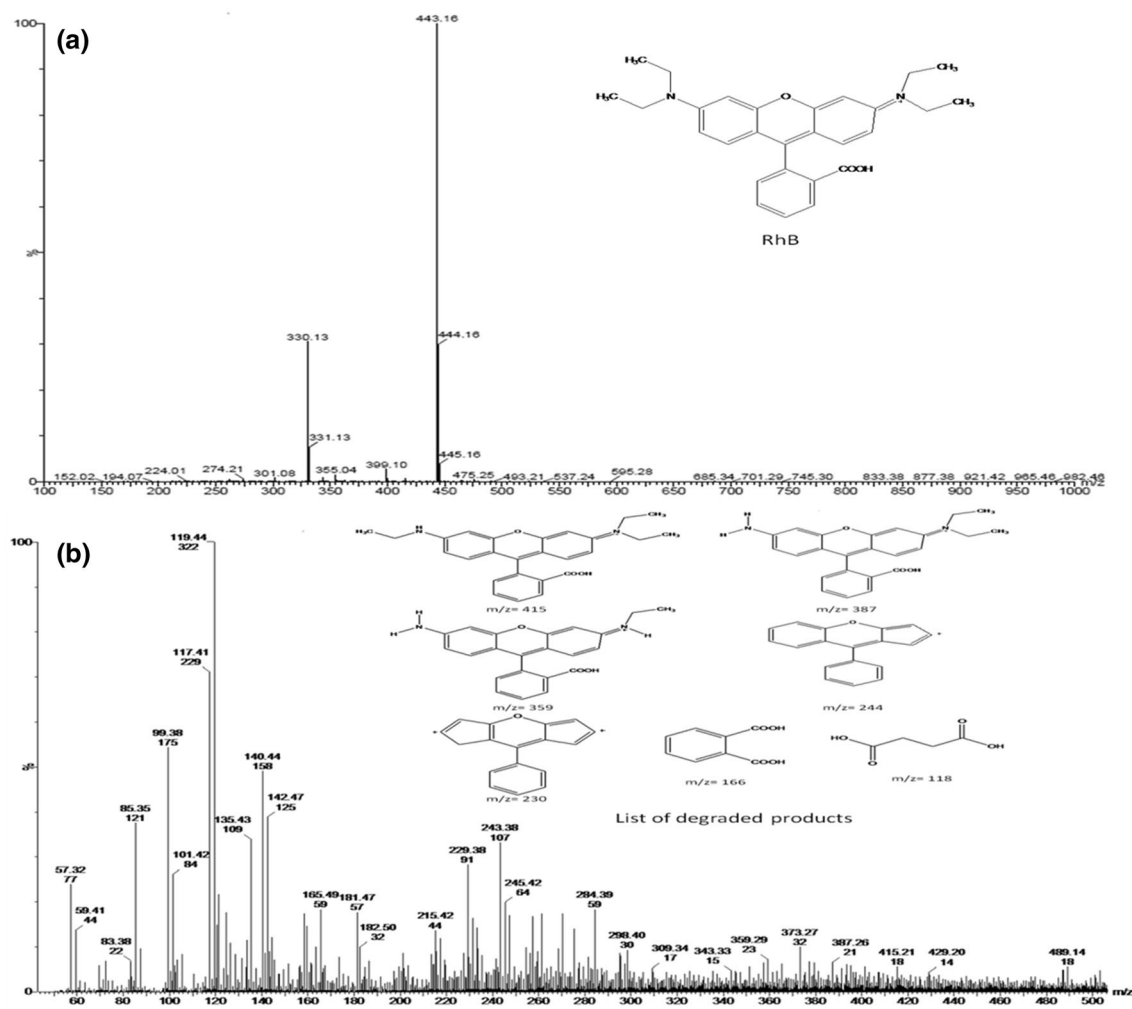
### Reduction of nitro compounds

Due the various applications of 4-aminophenol, the reduction of 4-nitrophenol to 4-aminophenol is considered as the benchmark system for the investigation of the catalytic activity of nanoparticles. Thus, the superior catalytic performance of the as-designed catalyst BiFeO<sub>3</sub> nanoparticles was thus estimated in the reduction of 4-nitrophenol (NP) to 4-aminophenol (AP) by using sodium borohydride (NaBH<sub>4</sub>) as a reducing agent or as hydrogen donor in aqueous media which is easily available and ecologically safe solvent. Various parameters such as type of catalyst as it was prepared by four different chelating agents, effect of calcination temperature, amount of catalyst, amount of NaBH<sub>4</sub>, concentration of 4-nitrophenol and different reaction conditions were applied on reduction experiments. In UV-Vis spectra, 4-nitrophenol (NP) showed a peak near 317 nm, with the addition of the freshly prepared NaBH<sub>4</sub> solution, a peak near 400 nm arised due to the formation of 4-nitrophenolate ion. This changed the color of the mixture from light yellow to bright yellow. When the catalyst was added to the reaction mixture, the intensity of the peak at 400 nm decreased and a fresh peak at 300 nm appeared

which confirms the successful formation of 4-aminophenol (AP) product as shown in Fig. 22.

The reduction experiment was performed by taking 5 ml of 4-nitrophenol (NP) (0.1 mmol), freshly prepared 12.5 ml of NaBH<sub>4</sub> (0.25 mmol) with 10 mg amount of BiFeO<sub>3</sub> nanoparticles prepared by different chelating agents (*W* without, *S* sucrose, *C* citric acid, *T* tartaric acid and *U* urea) calcinated at 650 °C. The mixture was stirred with appropriate time as shown in Fig. 21. The color of the mixture was initially light yellow; during reaction, it became bright yellow due to the formation of 4-nitrophenolate ion and finally became black color of 4 aminophenol. The better results were given by BiFeO<sub>3</sub> nanoparticles prepared by sucrose as a chelating agent on basis of least time, i.e., 6 m:13 s taken for the conversion as compared to others as illustrated in Fig. 23.

For the optimization of reaction condition, the reaction was tried at room temperature, under refluxing and sonication, by using fixed amount of catalyst (10 mg, BiFeO<sub>3</sub> nanoparticles prepared by sucrose as chelating agent and calcinated at 650 °C), NaBH<sub>4</sub> (0.25 mmol) and 4-nitrophenol (NP) (0.1 mmol). The time taken for the reduction experiment was found to be 6.13 min, 8.43 min and 9.39 min for room temperature, refluxing and sonication, respectively, as shown in Fig. 24. The findings confirm that reaction



**Fig. 20** Comparison study of mass spectroscopy of RhB **a** Before degradation, and **b** after degradation

complete fast at room temperature condition, which is cost-effective, energy efficient and green method according to environmental point of view.

After examining the best catalyst and reaction condition, our next aim was to evaluate the effect of calcination temperature on the reduction experiment. For this purpose, the reaction was tried under identical conditions of the substrate as discussed in earlier with BiFeO<sub>3</sub> prepared by sucrose as chelating agent and calcinated at 150 °C, 450 °C, 550 °C, 650 °C, 750 °C and 850 °C temperature, respectively. Among the all as-prepared catalysts, this conversion was better exhibited in least time by BiFeO<sub>3</sub> prepared at 650 °C as shown in Fig. 25. This could be due to the highest purity was exhibited by BiFeO<sub>3</sub> at this temperature. This observation was in good agreement with the previous results demonstrated by XRD analysis earlier.

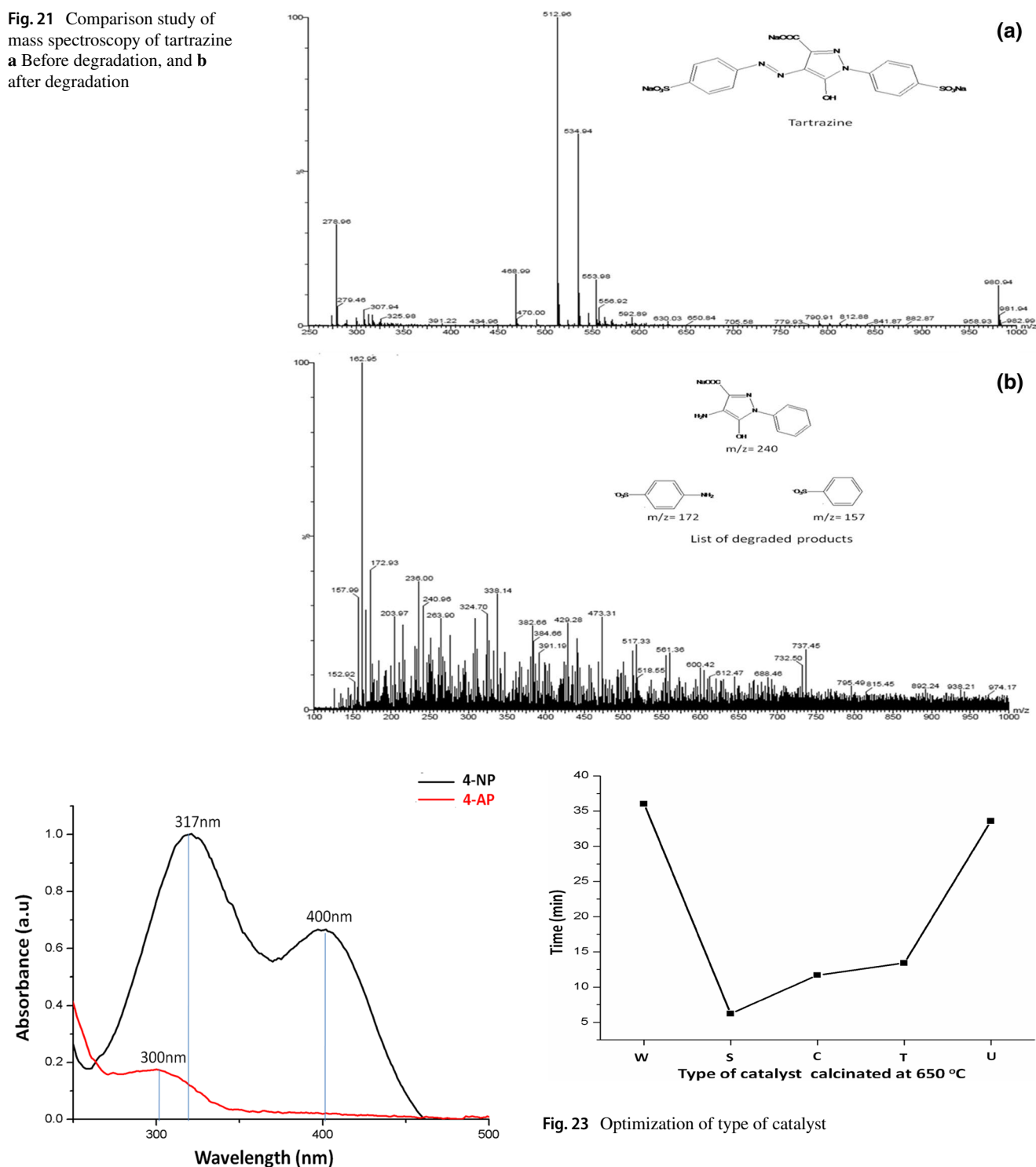
To optimized the better dose of catalyst, different amounts of BiFeO<sub>3</sub> nanoparticles such as 10 mg, 15 mg, 20 mg, 25 mg and 30 mg were explored on reduction experiment.

As we increased the catalytic amount from 10 to 25 mg, the conversion time decreased. The main reason is that as we increased the catalytic amount, the number of catalytic active sites increased which enhanced the reaction rate by decreasing time or we can say that due to proportional increment in number of catalytic active of the catalyst, activity of catalyst was increased [18]. However, no further improvement in conversion times was observed with increasing the amount, i.e., 30 mg. The more time taken in the initial amount could be due to more time taken for the diffusion of reactant to the catalytic surface, may be due oxidized surface and decreases in dissolved oxygen in solution [73]. These findings confirms that 25 mg load of catalyst was the optimized dose completing the conversion within 82 s as depicted in Table 4 (Entry 1-5).

In order to check, the applicability of as-prepared catalyst and use of NaBH<sub>4</sub> in reduction experiment. Firstly, reaction was tried without catalyst in the presence of NaBH<sub>4</sub>; conversion was not observed even for a long time due to the



**Fig. 21** Comparison study of mass spectroscopy of tartrazine  
**a** Before degradation, and **b** after degradation



**Fig. 22** UV-Vis spectra of reduction of 4-NP to 4-AP

repulsion between the 4-nitrophenol (NP) and  $\text{BH}_4^-$  ions. Secondly the reaction was also tried in the presence of catalyst without  $\text{NaBH}_4$ ; conversion did not occur at all. Thirdly reaction was tried with both using catalyst and  $\text{NaBH}_4$ ; conversion completes in seconds because catalyst facilitates the

**Fig. 23** Optimization of type of catalyst

electron relay system between the donor  $\text{BH}_4^-$  to acceptor 4-nitrophenol (NP) [59]. This confirms catalyst and reducing agent  $\text{NaBH}_4$  are essential for the effective reduction of the substrate [74] as demonstrated in Table 4 (Entry 4 and 6-7).

After finding the optimized load of catalyst, next study includes the use of different quantity of  $\text{NaBH}_4$ . Different quantities of  $\text{NaBH}_4$ , like 0.25 mmol, 0.53 mmol and 1.0 mmol had been tested by using the optimized amount

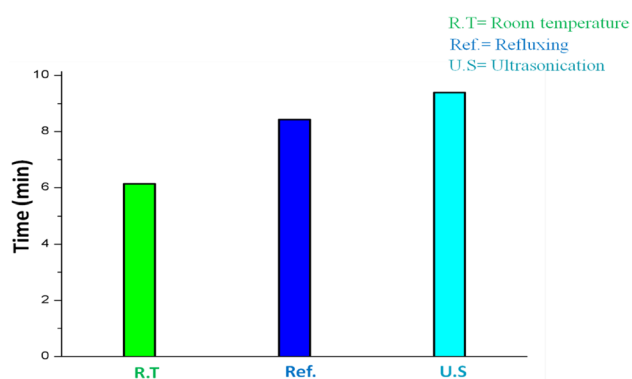


Fig. 24 optimization of reaction condition

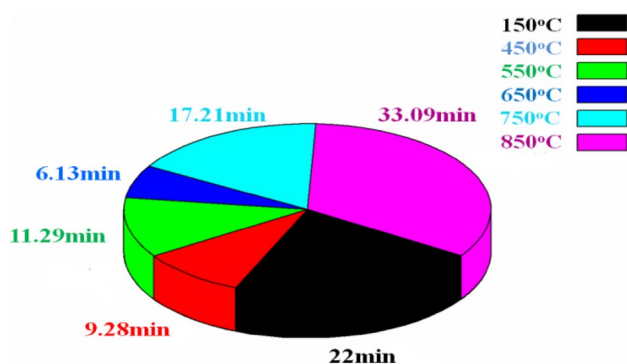


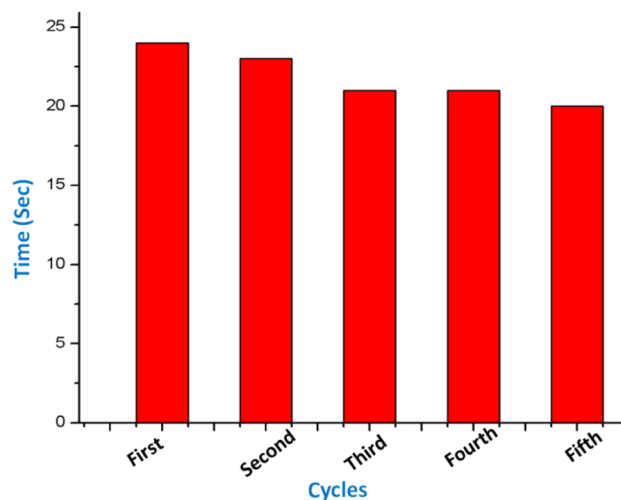
Fig. 25 Optimization of calcination temperature

of catalyst, i.e., 25 mg and fixed concentration of 4-nitrophenol (NP) (0.1 mmol). The reduction experiment was completed in 82 s, 24 s and 133 s for 0.25 mmol, 0.53 mmol and 1.0 mmol amount of  $\text{NaBH}_4$ , respectively, as in Table 4 (Entry 4, 8 and 9). The reaction rate increases with increasing

quantity of  $\text{NaBH}_4$ , because of increase in  $\text{BH}_4^-$  concentration [75]. This demonstrates that 0.53 mmol of  $\text{NaBH}_4$  was the sufficient amount to carry out the conversion.

Further various quantities of 4-nitrophenol (NP) like 0.1 mmol, 0.5 mmol and 1.0 mmol were investigated by using optimized amount of catalyst (25 mg) and  $\text{NaBH}_4$  (0.53 mmol). The reaction was completed in 24 s, 138 s and 446 s of 0.1 mmol, 0.5 mmol and 1.0 mmol for 4-nitrophenol (NP), respectively, as shown in Table 4 (Entry 8, 10 and 11).

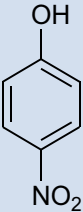
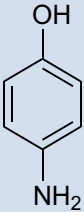

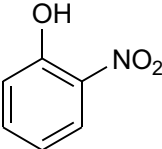
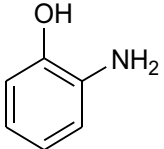
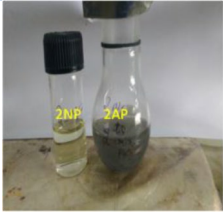
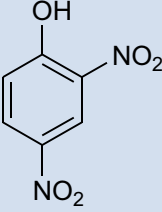
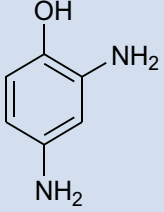
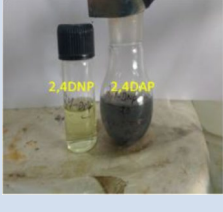
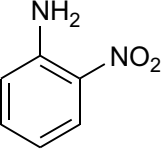
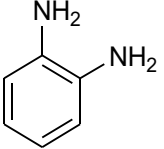

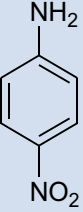
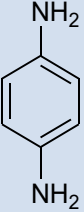

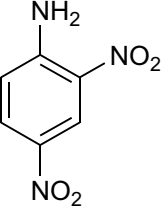
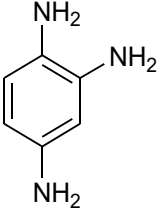

Further recyclability of the as-synthesized catalyst was demonstrated as shown in Fig. 26. The catalyst was recycled up to five cycles in the reduction experiment. It has been observed that there was no considerable loss in activity of the catalyst after being reused. This observation further confirmed the stability of the catalyst after recyclability.

Fig. 26 Recyclability of  $\text{BiFeO}_3$  nanoparticles in reduction experimentTable 4 Optimization of various reaction conditions<sup>a</sup>

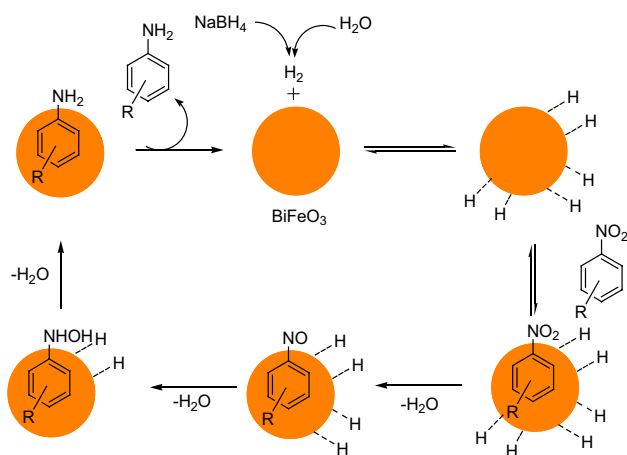
Entry	$\text{BiFeO}_3$ (mg)	$\text{NaBH}_4$ (mmol)	4-nitrophenol(NP) (mmol)	Time
1	10	0.25	0.1	6.13 min
2	15	0.25	0.1	5.19 min
3	20	0.25	0.1	5.14 min
4	25	0.25	0.1	82 s
5	30	0.25	0.1	6.02 min
6	25	–	0.1	No reaction
7	–	0.25	0.1	No reaction
8	25	0.53	0.1	24 s
9	25	1.0	0.1	133 s
10	25	0.53	0.5	138 s
11	25	0.53	1.0	446 s

Reaction conditions:  $\text{BiFeO}_3$  nanoparticles (mg) prepared by chelating agent Sucrose and calcinated at 650 °C, 12.5 ml of  $\text{NaBH}_4$  (mmol), 5 ml of 4-nitrophenol (NP) (mmol), RT room temperature, stirring at 800 rpm

**Table 5** Reduction of various nitro compounds with BiFeO<sub>3</sub> nanoparticles

S. No	Reactant	Product	Time (sec)	Conversion (%)	Variation in color
1.			24	100	
2.			33.03	100	
3.			6	100	
4.			20	100	
5.			33	100	
6.			58	100	

Reaction conditions: BiFeO<sub>3</sub> nanoparticles (25 mg) prepared by chelating agent Sucrose and calcinated at 650°C), 12.5 ml of NaBH<sub>4</sub> (0.53 mmol), 5 ml of 4-nitrocompound (0.1 mmol), RT room temperature, stirring at 800 rpm



**Scheme 4** Catalytic hydrogenation mechanism of nitro reduction

Based on the above observations, we explored the potential of this catalytic system, further the reduction of various nitro compounds was studied under optimized reaction condition, and the consequences are summarized in Table 5 and UV–Vis spectroscopy study in Fig. S1–S5 (supplementary data). The reduction of aromatic nitro compounds basically depends upon mainly two factors: (1) formation of intermediate (nitrophenolate ion) (2) and their reactivity. The formation of intermediate depends upon the acidic strength of aromatic nitro compounds where  $\text{NaBH}_4$  is a base. The order of acidic strength of nitrophenolate ion was found in the literature, i.e., 2,4-DNP > 4-NP > 2-NP [74]. Therefore, the reduction rate follows the same order (entry 1–3, Table 5). Further it has been observed that the reduction rate of 2,4-DNP was large as compared to aromatic nitroamines (entry 4–6, Table 5). The reason for this depends upon the electron donating power of amine group, i.e., decrease in electronegativity of nitrogen in aromatic amines as compared to oxygen of the hydroxyl group of aromatic nitrophenols and thus nitrophenolate ion [9].

### Mechanism of nitro reduction

Proposed mechanism of the reduction experiment proceeds through the following steps [17]: (1) during the course of the

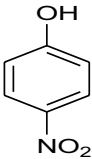
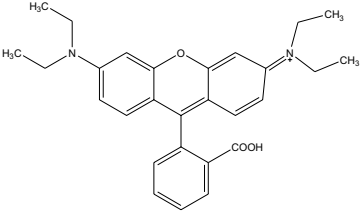
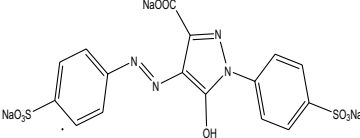
reaction  $\text{H}_2$  gas was produced, the reaction could be based on catalytic hydrogenation concept for the reduction of nitro group with  $\text{NaBH}_4$ ; (2) the effect of  $\text{BiFeO}_3$  nanoparticles could be due to the presence of Lewis acidic sites on the surface of the catalyst and hydride transformation from  $\text{NaBH}_4$ ; (3) solubility of  $\text{NaBH}_4$  in water followed by hydrolysis of the obtained amino-borane intermediates could be promoted the rate of reaction (Scheme 4).

After establishing, the catalytic system for the degradation of dye (RhB and tartrazine) and reduction of 4-nitro-compounds. Further we compared catalytic activity of as-prepared catalyst in both processes with the reported catalysts in the literature as illustrated in Table 6. It has been found that our developed method is much greener than others in case of cost-effective, simplicity, room temperature, use of water as medium and use of natural source of light, i.e., sunlight, which is abundantly available on earth. This proved the superiority of our present work.

### Conclusion

To sum up, we prepared perovskite-structured  $\text{BiFeO}_3$  nanoparticles by using different chelating agents (sucrose, citric acid, tartaric acid and urea) using auto-combustion route followed by calcination at different range of temperature, i.e., 150–850 °C. The selection of the better catalyst was carried out on the basis of their performance both in degradation and in reduction experiment.  $\text{BiFeO}_3$  nanoparticles prepared by using sucrose as chelating agent and calcinated at 650 °C have demonstrated a numerous promises in the terms of high activity, selectivity, chemical stability, recyclability, reusability, cost-effective, eco-friendly, degradation of organic contaminants and synthesis of fine chemicals. On the basis of their efficient photocatalytic activity, perovskite-structured  $\text{BiFeO}_3$  showed potentials for use in environmental purification of organic pollutants under natural sunlight and reduction of ANCs (aromatic nitro compounds) in aqueous medium at room temperature under stirring conditions and extend the scope of the photocatalyst in practical applications. Therefore, it would be the promising catalyst for the waste water treatment and chemical synthesis of important organic compounds.

**Table 6** Comparison Table of catalytic activity

Compound (process)	Catalytic system (Rex. condition)	Time	References
 4-NP (reduction)	Pd nanoparticles supported on reduced graphene oxide (NaBH <sub>4</sub> , EtOH-H <sub>2</sub> O, r.t)	120 min	[76]
 RhB(degradation)	Np-Ag-Al (NaBH <sub>4</sub> , H <sub>2</sub> O, r.t)	105 min	[77]
	NiFe <sub>2</sub> O <sub>4</sub> @Cu NPs(NaBH <sub>4</sub> , EtOH-H <sub>2</sub> O, reflux)	1 min	[17]
	IO@NiNPs(NaBH <sub>4</sub> , H <sub>2</sub> O, r.t)	10 min	[19]
	Nano-LaFeO <sub>3</sub> (KOH, (CH <sub>3</sub> ) <sub>2</sub> CHOH, MWI)	16 min	[78]
	Ag <sub>3</sub> PO <sub>4</sub> /CoFe <sub>2</sub> O <sub>4</sub> (NaBH <sub>4</sub> , r.t)	24 min	[79]
	np-Ag (NaBH <sub>4</sub> , EtOH-H <sub>2</sub> O, reflux)	105 min	[77]
	BiFeO <sub>3</sub> nanoparticles (NaBH <sub>4</sub> , H <sub>2</sub> O, r.t)	24 s	This work
 Tartrazine (degradation)	ZnO nanoparticles (UV illumination)	70 min	[80]
	H <sub>2</sub> Ti <sub>3</sub> O <sub>7</sub> nanotubes(UV irradiation)	630 min	[81]
	BiFeO <sub>3</sub> nanoparticles (Sunlight irradiation)	60 min	This work
	TiO <sub>2</sub> suspension (500 W superhigh pressure mercury)	117 min	[82]
	CuO (150 W Tungsten halogen lamp)	240 min	[83]
	BiFeO <sub>3</sub> nanoparticles (Sunlight irradiation)	60 min	This work

**Acknowledgements** We are thankful to IIT Ropar for Mass spectroscopy, CIL IIT Roorkee for VSM, BIT Bengaluru for BET, SAIF, Panjab University Chandigarh for TEM, Department of Chemistry NIT Jalandhar for FT-IR and UV-Vis spectroscopy. One of the authors (H.S) is thankful to UGC for providing the research fellowship. We would like to thank Miss Priya Arora and Miss Jigyasa Badhan for their valuable suggestions in the manuscript writing.

## References

- Z. Yang, Y. Ma, Y. Liu, Q. Li, Z. Zhou, Z. Ren, Chem. Eng. J. **315**, 403 (2017)
- T. Soltani, M.H. Entezari, Chem. Eng. J. **223**, 145 (2013)
- H. Kusic, I. Petermel, S. Ukic, N. Koprivanac, T. Bolanca, S. Papic, Chem. Eng. J. **172**, 109 (2011)
- O.A. Attallah, M.A. Al-ghobashy, M.Y. Salem, RSC Adv. **6**, 11461 (2016)
- R. Nagaraja, N. Kottam, C.R. Girija, B.M. Nagabhushana, Powder Technol. **215**, 91 (2012)
- L. You-ji, C. Wei, Catal. Sci. Technol. **1**, 802 (2011)
- D. Gudovan, A. Fica, D. Fica, B.S. Vasile, M. Science **10**, 1329 (2015)
- A. Jodat, Water Treat. **52**, 2668 (2014)
- G. Singh, S. Rani, A. Arora, Sanchita, H. Duggal, D. Mehta, Mol. Catal. **431**, 15 (2017)
- N.M. Shooshtari, M.M. Ghazi, Chem. Eng. J. **315**, 527 (2017)
- R.M. Mohamed, I.A. Mkhallid, E.S. Baeissa, J. Nanotechnol. **1**, 5 (2012)
- T. Gao, Z. Chen, Y. Zhu, F. Niu, Q. Huang, L. Qin, Mater. Res. Bull. **59**, 6 (2014)
- L.M. Cotoruelo, M.D. Marqués, F.J. Díaz, J. Rodríguez-Mirasol, J.J. Rodríguez, T. Cordero, Chem. Eng. J. **184**, 176 (2012)



14. A.G. Karunanayake, O.A. Todd, M.L. Crowley, L.B. Ricchetti, C.U. Pittman, R. Anderson, *Chem. Eng. J.* **319**, 75 (2017)
15. A. Hernández-Gordillo, V.R. González, *Chem. Eng. J.* **261**, 53 (2015)
16. V.S. Kirankumar, S. Sumathi, *Mater. Res. Bull.* **93**, 74 (2017)
17. B. Zeynizadeh, I. Mohammadzadeh, Z. Shokri, S.A. Hosseini, *J. Colloid Interface Sci.* **500**, 285 (2017)
18. S.F.N. Rashidi, *J. Iran. Chem. Soc.* **6**, 1021 (2012)
19. P.S. Rathore, R. Patidar, T. Shripathi, S. Thakore, *Catal. Sci. Technol.* **22**, 286–295 (2014)
20. S. Sumathi, V. Lakshmi Priya, *J. Mater. Sci.: Mater. Electron.* **28**, 2795 (2017)
21. M. Kumarraja, K. Pitchumani, *Appl. Catal. A Gen.* **265**, 135 (2004)
22. T. Soltani, M.H. Entezari, *Ultrason. Sonochem.* **20**, 1245 (2013)
23. G. Singh, V.S. Tiwari, P. Tiwari, A.K. Srivastava, P.K. Gupta, *J. Alloys Compd.* **509**, 4127 (2011)
24. M.A. Aghayan, M.A. Rodríguez, *Mater. Sci. Eng., C* **32**, 2464 (2012)
25. H. Singh, J.K. Rajput, *J. Mater. Sci.* **53**, 3163 (2018)
26. S. Farhadi, M. Zaidi, *J. Mol. Catal. A: Chem.* **299**, 18 (2009)
27. Y. Wang, Y. Hu, L. Fei, Y. Zhang, J. Yuan, H. Gu, *J. Nanomater.* **2011**, 797639 (2011)
28. M. Arora, P.C. Sati, S. Chauhan, S. Chhoker, A.K. Panwar, M. Kumar, *J. Supercond. Nov. Magn.* **26**, 443 (2013)
29. S. Chakraborty, S. Mukherjee, *J. Aust. Ceram. Soc.* **51**, 45 (2015)
30. N. Das, R. Majumdar, A. Sen, H.S. Maiti, *Mater. Lett.* **61**, 2100 (2007)
31. F. Gao, X. Chen, K. Yin, S. Dong, Z. Ren, F. Yuan, *Adv. Mater.* **19**, 2889 (2007)
32. A. Manzoor, A.M. Afzal, M. Umair, A. Ali, M. Rizwan, M.Z. Yaqoob, *J. Magn. Magn. Mater.* **393**, 269 (2015)
33. D.K. Palchaev, M.P. Faradzheva, S.A. Sadykov, M.K. Rabadanov, Z.K. Murlieva, S.N. Kallaev, *Tech. Phys. Lett.* **40**, 961 (2014)
34. B. Bhushan, A. Basumallick, S.K. Bandopadhyay, N.Y. Vasantacharya, D. Das, *J. Phys. D Appl. Phys.* **42**, 65004 (2009)
35. C. Fu, M. Huo, W. Cai, X. Deng, *J. Ceram. Process. Res.* **13**(561), 561 (2012)
36. J. Lu, L.J. Qiao, P.Z. Fu, Y.C. Wu, *318*, 936 (2011)
37. Y. Hu, L. Fei, Y. Zhang, J. Yuan, Y. Wang, *J. Nanometer*, 797639 (2011)
38. A. Maleki, R. Rahimi, S. Maleki, *Synth. Met.* **194**, 11 (2014)
39. H. Shokrollahi, *Magnetic. Powder Technol.* **235**, 953 (2013)
40. J.L. Ortiz-Quirón, D. Díaz, I. Zumeta-Dubé, H. Arriola-Santamaria, I. Betancourt, P. Santiago-Jacinto, *Inorg. Chem.* **52**, 10306 (2013)
41. M. Ea, A. Sm, B. Yo, K. Cd, *J. Mater. Sci. Eng.* **5**, 3 (2016)
42. J.P. Singh, R.C. Srivastava, H.M. Agrawal, *A.I.P. Conf. Proc.* **1276**, 137 (2010)
43. B.S. Avinash, V.S. Chaturmukha, H.S. Jayanna, C.S. Naveen, M.P. Rajeeva, B.M. Harish, *AIP*, **20426** (2016)
44. T. Soltani, M.H. Entezari, *J. Mol. Catal. A: Chem.* **377**, 197 (2013)
45. K. Varunkumar, R. Hussain, G. Hegde, A.S. Ethiraj, *Mater. Sci. Semicond. Process.* **66**, 149 (2017)
46. H. Singh, J.K. Rajput, G. Govil, P. Arora, J. Badhan, *Appl. Organomet. Chem.* **32**, 1 (2018)
47. M.V. Lopez-Ramon, F. Stoeckli, C. Moreno-Castilla, F. Carrasco-Marin, *Carbon* **37**, 1215 (1999)
48. R.C. Meena, *Int. Res. J. Environ. Sci.* **2**, 35 (2013)
49. H. Atiqah, M. Azmy, N.A. Razuki, A.W. Aziz, *J. Phys. Sci.* **28**, 85 (2017)
50. K. Nagaveni, G. Sivalingam, M.S. Hegde, G. Madras, *Appl. Catal. B Environ.* **48**, 83 (2004)
51. A.P. Toor, A. Verma, C.K. Jotshi, P.K. Bajpai, V. Singh, *Dye. Pigment.* **68**, 53 (2006)
52. W. Bahnemann, M. Muneer, M.M. Haque, *Catal. Today* **124**, 133 (2007)
53. N. Daneshvar, D. Salari, A.R. Khataee, *J. Photochem Photobiol A Chem.* **157**, 111 (2003)
54. A.R. Khataee, M. Fathinia, S. Aber, M. Zarei, *J. Hazard. Mater.* **181**, 886 (2010)
55. W. Luo, L. Zhu, N. Wang, H. Tang, M. Cao, Y. She, *Environ. Sci. Technol.* **44**, 1786 (2010)
56. M. Movahedi, A.R. Mahjoub, S. Janitabar-Darzi, *J. Iran. Chem. Soc.* **6**, 570 (2009)
57. P. Arora, A. Fermah, J.K. Rajput, H. Singh, J. Badhan, *Environ. Sci. Pollut. Res.* **24**, 19546 (2017)
58. M. Montazerzohori, Y. Branch, *Environ. Prot. Eng.* **38**, 45–55 (2012)
59. A.K. Abay, X. Chen, D.-H. Kuo, *New J. Chem.* **41**, 5628 (2017)
60. J. Tang, R. Wang, M. Liu, Z. Zhang, Y. Song, S. Xue, *Chem. Eng. J.* **351**, 1056 (2018)
61. J. Wang, G. Zhang, Z. Zhang, X. Zhang, G. Zhao, F. Wen, *Water Res.* **40**, 2143 (2006)
62. Z. Lu, Z. Yu, J. Dong, M. Song, Y. Liu, X. Liu, *Chem. Eng. J.* **337**, 228 (2018)
63. Y. Wang, G. Tan, T. Liu, Y. Su, H. Ren, X. Zhang, *Appl. Catal. B Environ.* **234**, 37 (2018)
64. H. Dong, J. Sun, G. Chen, C. Li, Y. Hu, C. Lv, *Phys. Chem. Chem. Phys.* **16**, 23915 (2014)
65. S.P. Pattnaik, A. Behera, S. Martha, R. Acharya, K. Parida, *J. Nanoparticle Res.* **20**, 10 (2018)
66. H. Osman, Z. Su, X. Ma, *Environ. Chem. Lett.* **15**, 435 (2017)
67. M. Gobara, A. Baraka, *Int. Lett. Chem. Phys. Astron.* **33**, 106 (2014)
68. N. Serpone, *Environ. Sci. Technol.* **37**, 5813 (2003)
69. T. Rasheed, M. Bilal, H.M.N. Iqbal, S.Z.H. Shah, H. Hu, X. Zhang, *Environ. Technol.* **1**, 1533–1543 (2017)
70. D. Ariyanti, M. Maillot, W. Gao, *JECE* **6**, 539 (2018)
71. J.R. Steter, W.R.P. Barros, M.R.V. Lanza, A.J. Motheo, *Chemosphere* **117**, 200 (2014)
72. C. Ràfols, D. Barceló, *J. Chromatogr. A* **777**, 177 (1997)
73. L. Ai, H. Yue, J. Jiang, *J. Mater. Chem.* **22**, 23447 (2012)
74. A. Goyal, S. Bansal, P. Samuel, S. Singhal, *J. Mater. Chem. A Mater. Energy Sustain.* **2**, 18848 (2014)
75. A. Mondal, A. Mondal, B. Adhikary, *Bull. Mater. Sci.* **40**, 321 (2017)
76. W. Dong, S. Cheng, C. Feng, N. Shang, S. Gao, C. Wang, *Catal. Commun.* **90**, 70 (2017)
77. Z. Li, X. Xu, X. Jiang, Y. Li, Z. Yu, X. Zhang, *RSC Adv.* **5**, 30062 (2015)
78. S. Farhadi, F. Siadatnasab, *J. Mol. Catal. A: Chem.* **339**, 108 (2011)
79. E. Abroushan, S. Farhadi, A. Zabardasti, *RSC Adv.* **7**, 18293 (2017)
80. Q.I. Rahman, M. Ahmad, S.K. Misra, M. Lohani, *Mater. Lett.* **91**, 170 (2013)
81. S. Chatterjee, A.K. Tyagi, P. Ayyub, *J. Nanomater.* **2014**, 1 (2014)
82. K. Tanaka, K. Padermpole, T. Hisanaga, *Water Res.* **34**, 327 (2000)
83. M.P. Rao, J.J. Wu, A.M. Asiri, *Water Sci. Technol.* **75**, 1421 (2017)